Channel change during catastrophic flood: Example of Storm Alex in the Vésubie and Roya valleys

Frédéric Liébault, Gabriel Melun, Guillaume Piton, Margot Chapuis, Paul Passy, Sandrine Tacon

Geomorphology

Channel change during catastrophic flood: example of Storm Alex in the Vésubie and Roya valleys

--Manuscript Draft--

Manuscript Number:	GEOMOR-12938R1
Article Type:	VSI: Fluvial geomorphology
Keywords:	Fluvial metamorphosis; sediment wave; Extreme flood; Southern French Alps; storm Alex
Corresponding Author:	Frédéric Liébault University Grenoble Alpes FRANCE
First Author:	Frédéric Liébault
Order of Authors:	Frédéric Liébault
	Gabriel Melun
	Guillaume Piton
	Margot Chapuis
	Paul Passy
	Sandrine Tacon
Abstract:	Documenting and interpreting channel responses to catastrophic floods help understanding how rapid fluvial metamorphosis can propagate in a catchment under sediment cascading effects. The recent example of the October 2020 Storm Alex in SE France (~ 500 mm of rain in 24 h) provides a unique opportunity to investigate major geomorphic responses along 70 km of two confined alpine valleys (Vésubie and Roya) and to link them to sediment wave initiation and propagation. GIS-based analysis of remote sensing data (high-resolution ortho-imagery and airborne LiDAR data) acquired before and after the flood allowed combining channel changes with sediment erosion and deposition along a 35-km reach of the Vésubie, including the most impacted portions of the valley. In the Roya, the analysis was restricted to 2D morphological changes reconstructed with the sequence of ortho-imagery. Archives of aerial imagery were also used to integrate the storm impact in the historical trajectory of the rivers. The reconstruction of geomorphic responses shows a quasi-continuous fluvial metamorphosis along the investigated stream networks, with dramatic active channel widening and aggradation, having no antecedent analogs during the last 70 years in both valleys. The different glacial imprints between the two valleys is considered a key factor explaining the exacerbated channel response in the Vésubie, where a braided channel emerged along a 35-km river length. Many evidences strongly support that the fuelling effect of alluvial storage is a key element of the sediment cascade at the origin of the braided channel formation. This regional case study allows us to discuss the critical role of floodplain and terrace erosion in the formation of the post-flood braided channel, and to compare the geomorphic impact of the storm with similar reported cases in the literature.

Abstract

Documenting and interpreting channel responses to catastrophic floods help understanding how rapid fluvial metamorphosis can propagate in a catchment under sediment cascading effects. The recent example of the October 2020 Storm Alex in SE France (~ 500 mm of rain in 24 h) provides a unique opportunity to investigate major geomorphic responses along 70 km of two confined alpine valleys (Vésubie and Roya) and to link them to sediment wave initiation and propagation. GIS-based analysis of remote sensing data (high-resolution ortho-imagery and airborne LiDAR data) acquired before and after the flood allowed combining channel changes with sediment erosion and deposition along a 35-km reach of the Vésubie, including the most impacted portions of the valley. In the Roya, the analysis was restricted to 2D morphological changes reconstructed with the sequence of ortho-imagery. Archives of aerial imagery were also used to integrate the storm impact in the historical trajectory of the rivers. The reconstruction of geomorphic responses shows a quasi-continuous fluvial metamorphosis along the investigated stream networks, with dramatic active channel widening and aggradation, having no antecedent analogs during the last 70 years in both valleys. The different glacial imprints between the two valleys is considered a key factor explaining the exacerbated channel response in the Vésubie, where a braided channel emerged along a 35-km river length. Many evidences strongly support that the fuelling effect of alluvial storage is a key element of the sediment cascade at the origin of the braided channel formation. This regional case study allows us to discuss the critical role of floodplain and terrace erosion in the formation of the post-flood braided channel, and to compare the geomorphic impact of the storm with similar reported cases in the literature.

Keywords

Fluvial metamorphosis, sediment wave, extreme flood, Southern French Alps, Storm Alex

1. Introduction

The geomorphic effect of floods is a basic concern of fluvial geomorphology, insofar as processes of sediment transfer and redistribution during these events can produce major and persistent

morphological adjustments of river channels. Of particular interest is the geomorphic imprint of events with a magnitude far above extreme values of the contemporary flood regime (return periods > 100 yrs). These have been often referred to as catastrophic floods, with some demonstrative examples related to dam failures (Pitlick, 1993), rapid glacial melting during volcanic eruptions (Magilligan et al., 2002), glacial-lake outburst floods (Cenderelli and Wohl, 2003), and tropical convective or cyclone-driven rainfall cells (Croke et al., 2013; Milan et al., 2018; Heritage et al., 2019). It is often recognized that catastrophic floods generate a major transformation of alluvial landforms along important river lengths like the sudden interruption of multi-secular gradual floodplain accretion by the stripping effect of a flood related to channel widening (Nanson, 1986). Examples of flood-induced fluvial metamorphosis (*sensu* Schumm, 1969), like channel pattern shifting from single-thread to braiding, have also been reported (Arnaud-Fassetta et al., 2005; Rinaldi et al., 2016). However, the variability of morphological responses to floods for a given recurrence interval hinders determination of a critical return period associated with major geomorphic impacts (Magilligan et al. 1998). The maximum unit stream power of a flood offers a better predictor that takes into account local slope and valley floor confinement (Baker and Costa, 1987), a threshold value of 300 W m^{-2} having been proposed by Magilligan (1992) for a catastrophic flood to occur, but many other influential factors should be considered. A recent work addressing geomorphic effectiveness of debris floods in steepland streams has shown that the exceedance of the critical shear stress required to mobilize the coarse fraction of the bed material can be used to determine the magnitude of the channel response, this criterion being used to differentiate damaging and catastrophic debris floods (Church and Jakob, 2020). This emphasizes the importance of considering not only hydraulic forces generated by floods, but also channel resistance to disturbance (Brunsden, 2001; Milan, 2022). The geomorphic effectiveness of floods also depends on the climatic setting influencing the flashiness of the flow regime and the timescale of recovery (Wolman and Gerson, 1978), the recent flood history or memory of the fluvial system (Kochel, 1988), the duration of the flood (Costa and O'Connor, 1995), and the sediment supply conditions (Beschta, 1983).

The effect of sediment supply on geomorphic responses to extreme floods is particularly critical in mountain rivers and streams, due to their proximity to hillslope sediment sources. Hillslope-channel coupling controls the efficiency with which energy is transmitted through the fluvial system, explaining why sediment connectivity of upland catchments is recognized as a fundamental factor of their geomorphic sensitivity to disturbances (Brunsden, 2001; Harvey, 2001; Fryirs, 2013). Some recent major flood events in small mountain streams of the French Pyrenees (Blanpied et al., 2018) and Italian Alps (Pellegrini et al., 2021; Scorpio et al., 2022) illustrate how sediment connectivity can be used to reconstruct the sediment cascade associated with extreme events. The initiation and propagation of sediment waves is a classic geomorphic response to extreme floods in upland environments, with active channel widening and aggradation as the typical morphological imprints of the sediment wave (Beschta, 1983; Pitlick, 1993; Madej and Ozaki, 1996; Nelson and Dubé, 2016). In the case of the June 1957 catastrophic flood in the Guil valley of the Eastern French Alps, it has been early recognized that the remobilization of alluvial storages through local channel widening played a critical role in the downstream propagation of the sediment wave associated with this event (Tricart, 1960). This was supported by the lithological composition of alluvial deposits generated by the flood, showing relatively short displacements of individual grains during the flood. This early study echoes a more recent review of extreme sediment transport events, emphasizing the key role of sediment storage for "fuelling rather than buffering high sediment transport rates" (Korup, 2012). Fluvial terraces were also identified as the major sediment source during an extreme flood in a small upland catchment of Northern England (Milan, 2012).

From a more practical perspective related to the prevention against flooding hazards in upland environments, it is crucial to better characterize controlling factors of the channel response to extreme floods. Of particular importance is the width ratio, computed as the ratio between the post-flood and the pre-flood active channel width. This widely-used normalized index is crucial for management strategies based on a functional river corridor width ensuring at the same time a protection against channel shifting during floods, and the preservation of the ecological quality of the river (Piégay et al., 2005). The occurrence of many extreme flood events in upland environments of Europe during the last

two decades gave rise to many case studies dedicated to width ratios. It was notably shown that the widening rate at the reach scale depends not only on the specific stream power of the flood, but also on local factors such as the initial channel width or the channel confinement in the valley floor (Krapesch et al 2011; Rinaldi et al., 2016; Surian et al.; 2016; Righini et al., 2017; Lucia et al., 2018; Scorpio et al., 2018; Ruiz-Villanueva et al., 2018; Scorpio et al., 2022; Brenna et al., 2023).

In early October 2020, a catastrophic flood occurred in several confined alpine valleys of SE France. This flood was generated by a Mediterranean episode subsequent to a storm coming from North Atlantic, known as the Storm Alex (Carrega and Michelot, 2021). Geomorphic responses to the storm have been particularly dramatic in the Vésubie and the Roya valleys, where valley floors have been buried under massive gravel depositions. This major geomorphic event offers a unique opportunity to investigate how a sediment disaster may occur in alpine valleys under the effect of extreme meteorological forcings. A detailed analysis of the sediment cascade and associated geomorphic response was done using airborne remote sensing data, with several specific objectives: (1) documenting the morphological imprint of the storm and contextualizing it within the recent historical trajectories of the rivers; (2) analyzing the spatial variability of reach-scale channel responses; (3) comparing the morphological responses of the two rivers; (4) and interpreting sediment cascading effects using available information on the geomorphic response.

2. Physical setting

2.1. Vésubie and Roya valleys

The Vésubie and Roya are two neighboring alpine gravel-bed rivers of SE France, draining the southeastern flank of the Argentera-Mercantour mountain range, in the hinterland of the city of Nice, with respective drainage areas of 392 and 671 km² (Fig. 1). The Vésubie is a left-bank tributary to the Var River that joins the Mediterranean Sea close to Nice, while the Roya flows directly to the sea at Ventimiglia (Italy). A 36-km study reach has been considered for the Roya, from the upper valley down to the Italian border (Fig. 1). Channel slope is decreasing from 10% to 1% along this reach. The 35-km study reach considered for the Vésubie catchment is divided into three sub-reaches (Fig. 1): (1)

the Boréon between the confluence with the Vallon de Salèse down to the confluence with the Vésubie (length of 6.8 km, mean channel slope of 6.7%); (2) the Upper Vésubie (also known locally as Madone de Fenestre) from the confluence with the Vallon de Prals down to the confluence with the Boréon (length of 8.9 km, mean channel slope of 8.7%); and (3) the Vésubie from the confluence with the Boréon down to the upstream end of the narrow gorges present in the lower valley (length of 19.5 km, mean channel slope of 3%). Predominant channel morphology for these rivers before Storm Alex was a single-thread pattern with only few exposed gravel bars.

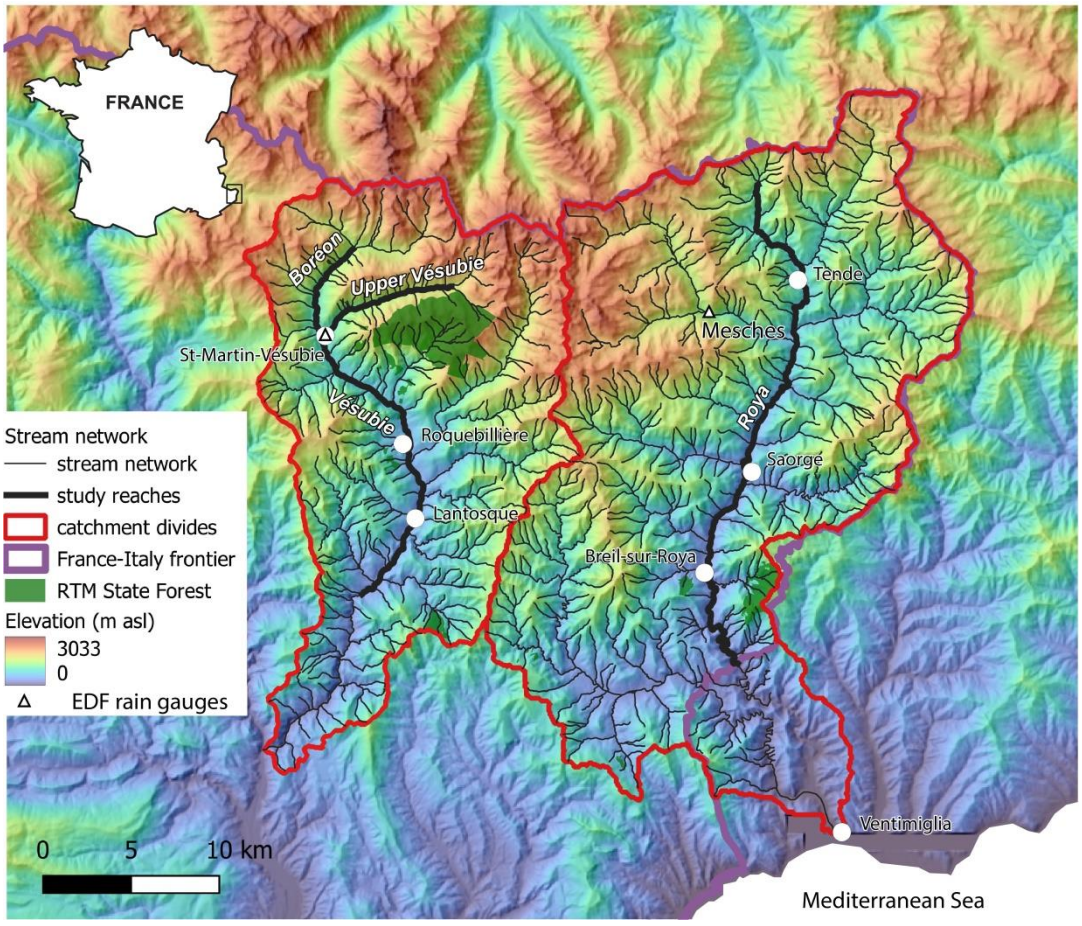

Figure 1. General relief map of Vésubie and Roya river basins in the Southern French Alps, with localization of the study reaches. RTM State Forests correspond to land purchased by the State in the late 19th century for erosion-control works. White dots correspond to main villages.

Although the two catchments share several features related to their common physical setting, they also have some specificities (Tab. 1). Geology of the two catchments comprised both crystalline and

sedimentary rocks, but the proportion of crystalline rocks is much higher in the Vésubie, where the upper sub-catchments are composed quasi-exclusively of geological formations from the granitic basement of the Southwestern Alps (Fig. 2). Crystalline rocks are also present in the Upper Roya, but only marginally in its northwestern part. The major part of the Roya catchment as well as the middle and lower parts of the Vésubie catchment belongs to the Mesozoic and Cenozoic sedimentary domains, with dominant rock types like limestones, sandstones, and marls.

Upper catchments were glaciated during Pleistocene cold periods, and massive glacial deposits are present along many upper valleys. Imprints from cold periods are important to consider since they can have a significant effect on present-day sediment sources and stores of fluvial systems. Reconstructions of maximum glacier extensions during the Würm show that the main valley of the Vésubie down to Lantosque was glaciated, while most of the Roya valley stayed unglaciated (Julian, 1997). The spatial extent of alluvial deposits (fluvio-glacial terraces and recent floodplain) is reflecting that, these being much more extended in the Vésubie, notably in the upper and middle portions of the valley (Fig. 2). Massive fluvio-glacial deposits found in the Vésubie between Roquebillière and Saint-Martin-Vésubie have been interpreted as a consequence of the valley obstruction by the Gordolasque glacier during the last glacial retreat (Julian, 1997). Fluvio-glacial deposits are extremely limited in the Roya valley, where the river flows through narrow proglacial gorges along almost all of its course. Confined proglacial gorges are also present in the Vésubie, but they are mainly developed along the lower river course.

Both catchments are characterized by widespread forest stands, covering around 60% of drainage areas (Tab. 1). If other vegetation types are considered (open forest, shrub, and herbaceous covers), total vegetated proportions of the catchments reach 94% and 89% for the Roya and Vésubie, respectively. This not only shows a relatively small present-day agricultural pressure in both catchments, restricted to gentle slope areas near villages, but also a limited spatial extension of active erosion landforms on hillslopes, representing less than 6% and 11% of drainage areas for the Roya and Vésubie, respectively. It is also interesting to see that surfaces of RTM (*Restauration des Terrains en*

171 *Montagne*) State Forests are relatively limited (Fig. 1). They represent only 1% and 6% of catchment
172 areas for the Roya and Vésubie, respectively. These correspond to degraded lands purchased by the
173 State in the late 19th century to implement erosion-control works (Liébault et al., 2005; Piton et al.,
174 2017), and they provide a first indication of past erosion conditions on hillslopes.
175

Study sites	Roya	Vésubie
Drainage area (km²)	671	392
Mean active channel width (m)*	15.4 (7.4)	19.1 (8.9)
Mean elevation (m)	1235	1445
Maximum elevation (m)	2935	3143
Area above 1000 m (%)	63	71
Mean catchment slope (°)	27	28
Mean annual rainfall (mm)	1162	1339
Forest cover (%)	63	62
Open forest, shrub, and herbaceous vegetation (%)	31	27
Other land-uses (%)	6	11
RTM State Forests (%)	1	6
Crystalline rocks (%)	3	21
Sedimentary rocks (%)	74	50
Colluvium (%)	18	20
Glacial deposits (%)	4	6
Alluvium (%)	1	3

176 * computed for the study reaches, standard deviation in brackets

177 Table 1. Main physical features of the Roya and Vésubie catchments and study reaches. Active channel widths
178 correspond to mean values extracted from 2017 ortho-images along study reaches (see sections 3.2 and 3.3).
179 Relief features were extracted from 75-m resolution DEM from IGN (BD ALTI). Mean annual rainfall computed
180 from SPAZM reanalysis for the 1970-1999 period (Gottardi et al. 2012). Geological features were extracted from
181 1/50 000 digital geological maps from BRGM (BD Charm-50); the geology of the Italian part of the Roya
182 catchment was not considered in the analysis. Land-use was extracted from the IGN BD Forêt V2 providing a
183 classification of the vegetation cover in France (the forest cover include all polygons classified as closed forest in
184 the IGN nomenclature); the land-use of the Italian part of the Roya catchment was not considered in the analysis.
185

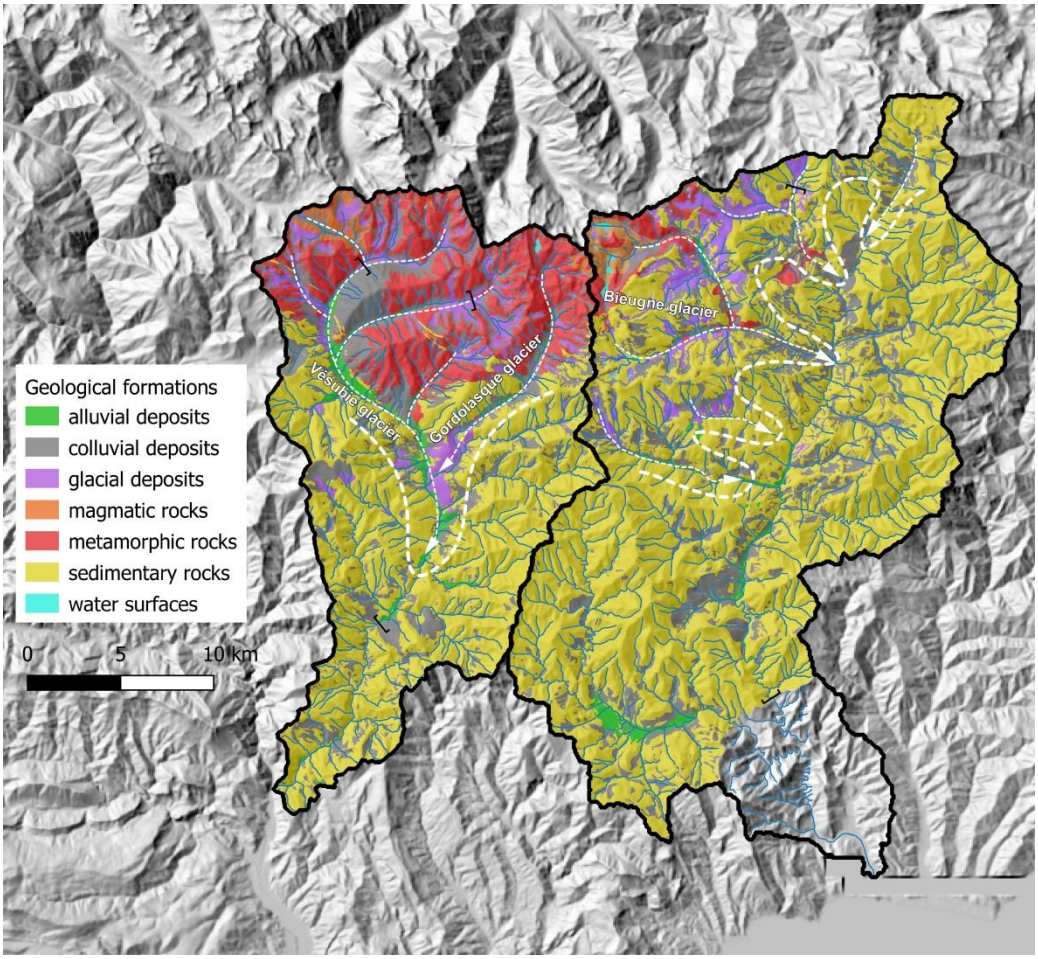

Figure 2. Geology and glacial imprints of the Roya and Vésubie catchments; geological formations classified from 1/50 000 digital geological maps from BRGM (BD Charm-50). Maximum glacier extensions during the Würm (white dotted lines) adapted from Julian (1997). Black square brackets correspond to upper and lower limits of study reaches.

2.2. October 2020 Storm Alex

Alex is the name given by Météo France (in partnership with national weather services of Spain, Portugal and Belgium) to a meteorological storm generated by the rapid formation of a cyclonic depression in North Atlantic, at around 600 km from Brittany (NE France), the 1st October 2020. This depression reached Brittany on October 2nd, and generated a southern flux of warm and humid air mass coming from the Mediterranean Sea, that induced an extreme rainfall episode in the Alpes-Maritimes (SE edge of France). The 24h Météo France rainfall map computed from radar data shows two rainfall hotspots of 600 and 500 mm in the upper catchments of the Roya and Vésubie rivers, respectively (Fig. 3). Rain gauges from EDF located at Saint-Martin-Vésubie and at Les Mesches

(Upper Roya) provided values of 502 and 633 mm in 24h, respectively. The return period of these rainfall amounts estimated from a statistical analysis is >1000 yrs (Cerema, 2021). This Mediterranean episode generated catastrophic floods in the two catchments. There is a lack of data on peak discharges, because gauging stations were destroyed during the flood, but field surveys of hydraulic sections using flood marks combined with hydrological modelling provided a range of possible peak discharges, with values comprised between 700 and 1100 m^3/s for the Vésubie at its mouth, and between 1100 and 1800 m^3/s for the Roya at the Italian border (Payrastre et al., 2022). Return periods associated with these peak discharges are comprised between 100 and 500 years. The relatively long duration of the floods, 18 to 24 hours (Cerema, 2021), likely contributed to their dramatic morphological effects. Reconstructed peak discharges of Storm Alex for both rivers are not only much higher than annual maximum daily peak discharges obtained from relatively short hydrological time series of gauging stations, but also much higher than all the estimated peak discharges of known historical floods of the 20^{th} century (Fig. 4). However, information is missing for comparing the magnitude of the Storm Alex flood with older historical floods from the second half of the 19^{th} century, whose impacts were sufficiently important to have left traces in the historical archives. Like Storm Alex, those old damaging large floods systematically occurred during autumn : November 1856, October 1882, October 1892, and November 1906 (Fig. 4).

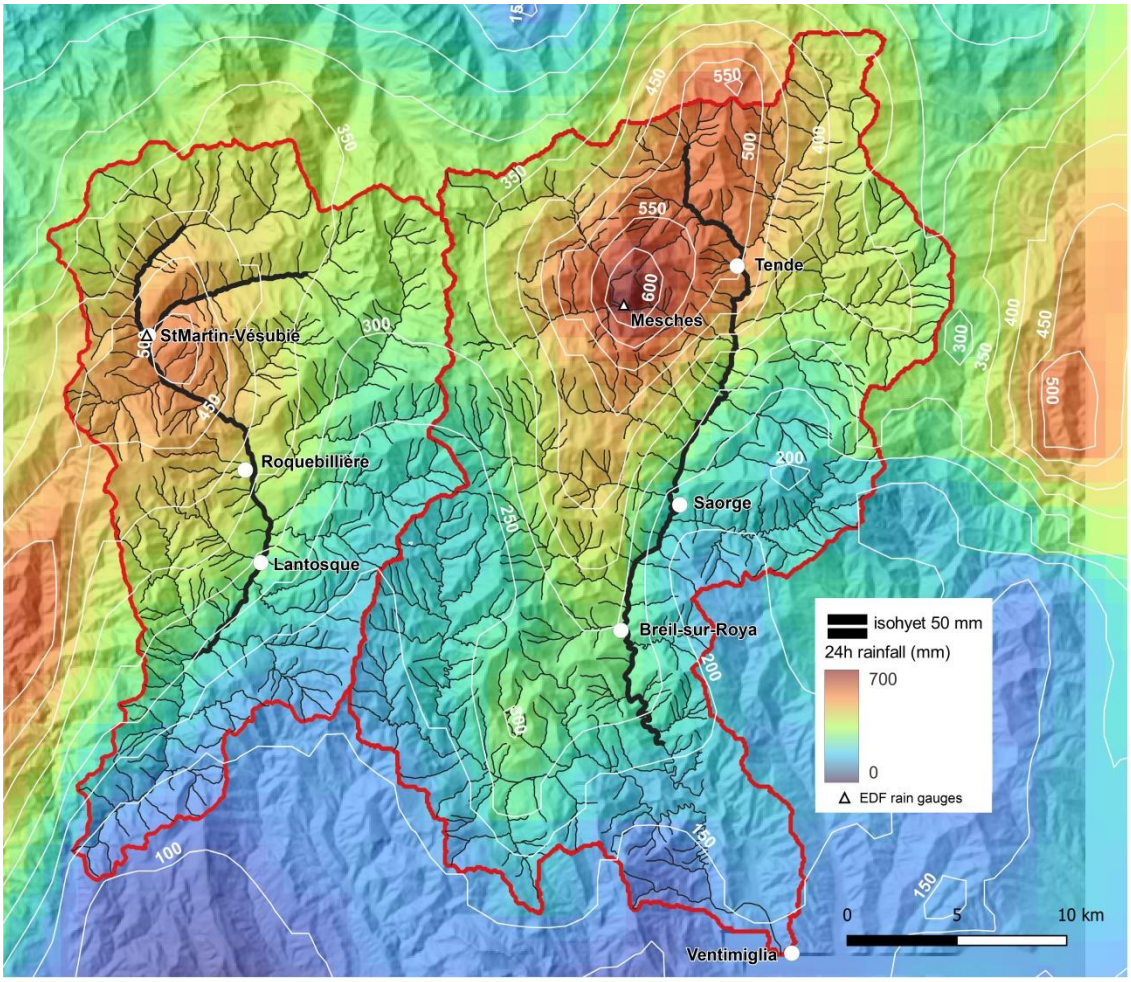

Figure 3. 24h rainfall map produced from the fusion of radar and rain gauge data for the time interval comprised between 02/10/2020 06:00 UTC and 03/10/2020 06:00 UTC (Météo France ANTILOPE rainfall database reanalyzed by EDF). Catchment divides appear in red, the stream network in thin black lines, study reaches in thick black lines.

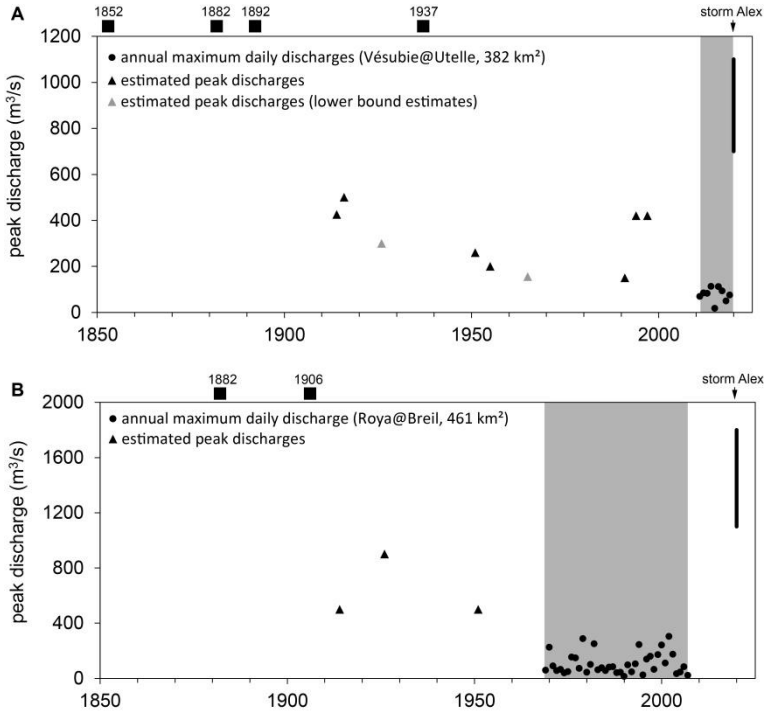

Figure 4. Estimated peak discharges of Storm Alex in the recent flood history of the Vésubie (A) and Roya (B). Periods of hydrological recording from gauging stations appear in grey (data from https://hydro.eaufrance.fr/). Estimated peak discharges of ungauged large floods (triangles) and years of known large floods from historical archives (black squares) have been obtained from ONF-RTM-INRAE (2022 a and b).

3. Material and methods

3.1. Remote sensing data

The documentation of the Storm Alex consequences remarkably benefited from an express IGN aerial survey that was undertaken only 3 days after the disaster to evaluate damages and impacted areas, following a request from local authorities in charge of natural hazard management (DDTM and ONF-RTM of the Alpes-Maritimes). More than 2000 aerial images combined with airborne LiDAR data were captured between the 5th and 7th October 2020. These remote sensing data were rapidly shared in a dedicated web site (https://www.geoportail.gouv.fr/donnees/ortho-express-alex), allowing an early exploitation for the geomorphic study.

The channel response to Storm Alex and its integration into the recent trajectory of the rivers have been investigated through a classical exploitation of available remote sensing data (Tab. 2). Seven sets

242 of high-resolution ortho-images were used for the Vésubie, and only 4 sets for the Roya. The lower
243 investigation effort for the Roya is justified by a lower morphological activity related to the strong
244 lateral confinement of the river. These raster datasets are in open-access from the web servers of data
245 providers (IGN and CRIGE PACA), except for the 1995 imagery. The lack of ortho-images between
246 1948 and 1999 in the Vésubie was compensated by the photogrammetric processing of 1995 aerial
247 photographs available from the dedicated IGN website (https://remonterletemps.ign.fr/). Many other
248 aerial campaigns are available for the Vésubie, but the meticulous inspection of channel evolution
249 between 1948 and 1995 did not reveal any significant morphological activity. The inclusion of the
250 1995 aerial dataset is justified by the occurrence of a major flood in the Vésubie in November 1997
251 (c.a. 100-yr return period at Roquebillière). Photogrammetric processing was done with the Structure
252 from Motion (SfM) program Agisoft Metashape (version 1.6.2). The planimetric accuracy of the SfM
253 ortho-image was improved by a georectification using control points in the valley floor that can be
254 detected in both the 1995 and 2020 ortho-images. This last processing step was done with the QGIS
255 georeferencing function.
256
257 In complement to ortho-imagery, two airborne near-infrared LiDAR surveys were available in the
258 Vésubie for undertaking a topographic differencing analysis of the Storm Alex. Unfortunately, only
259 the post-Alex LiDAR survey is available for the Roya, making impossible to duplicate the analysis for
260 both rivers. Post-Alex surveys were not only used for topographic differencing, but also for
261 morphological mapping of the modern valley floors and post-flood active channels for both rivers (see
262 next section). Near-infrared LiDAR data are restricted to terrestrial portions of the surveyed areas and
263 cannot provide bathymetric topography. This implies some limitations for topographic differencing
264 (see section 3.4), but not for morphological mapping.
265

Dates	Types	Resolution (m)	Dates of aerial campaigns	Sources	Study sites
1948	ortho-images (black and white)	0.50	23/08/1948	BD-ORTHO-Historique IGN	Roya, Vésubie
1995	aerial photos		25-26/06/1995	IGN (1995-FD06/200)	Vésubie
1999	ortho-images (color)	0.50	04-05/06/1999	BD-ORTHO IGN	Vésubie
2004	ortho-images	0.50	09-26/06/2004	BD-ORTHO IGN	Vésubie

	(color)				
2009	ortho-images (color)	0.20	28/05 – 30/07/2009	G0-06 / CRIGE PACA / Aérodata	Roya, Vésubie
2017	ortho-images (color)	0.20	13/06/2017 05-06/07/2017	BD-ORTHO-HR IGN	Roya, Vésubie
2018	LiDAR DEM (near infrared)	0.50 (7.9)*	07-29/11/2018	Sintegra / Métropole Nice Côte d'Azur	Vésubie
2020	ortho-images (color)	0.10	05-07/10/2020	ORTHO-EXPRESS IGN	Roya, Vésubie
2020	LiDAR DEM (near infrared)	0.50 (3.5)*	05-07/10/2020	IGN	Roya, Vésubie

* values in brackets correspond to average densities of 3D point clouds classified as ground points (number of points / m²)

Table 2. Remote sensing data used for 2D morphological mapping and topographic differencing

3.2. Active channel and modern valley floor mapping

Extraction of active channel was done manually by an expert-based photointerpretation mapping using QGIS. A single operator did this task for the seven dates of the Vésubie to avoid as much as possible an operator bias in active channel mapping. It was not possible to follow this rule for the Roya, where extraction was done by two operators. However, common mapping guidelines were shared between operators to avoid major interpretation differences. Areas considered as part of the active channel include low-flow channels, unvegetated gravel bars, and gravel bars occupied by sparse vegetation (Fig. 5A). Wooded islands have been excluded when their size exceeds about 150 m², for practical reason (saving time during manual digitizing of active channels). Areas in the margins of the floodplain showing clear flooding marks, like overbank accumulations of fine sediments and/or large woods, were also excluded (Fig. 5B). These mapping rules are justified by the most commonly used definition of active channel as a temporary storage of the coarse sediment load of a river that is frequently mobilized (or has been recently mobilized) by flow events (Williams and Rust, 1969; Liébault and Piégay, 2002; Haschenburger and Cowie, 2009). The combined used of ortho-images and LiDAR Digital Elevation Model (DEM) was particularly useful for post-Alex active channel extraction, because in some places, it was uneasy to map the limit between alluvial bars and destabilized banks or talus slopes based on ortho-images alone. This was much easier by looking at the post-Alex LiDAR derived slope raster (Fig. 5C and D). The ante-Alex slope raster obtained from the 2018 LiDAR survey (MNS LIDAR25cm©SIGMNCA obtained courtesy of the *Métropole de Nice*) was also very useful for improving extraction along narrow river reaches where the active channel was

masked by riparian vegetation (Fig. 5 E and F). Those instances were mostly encountered in the upper reaches of the Vésubie catchment before Storm Alex (Madone de Fenestre and Boréon valleys). It was not possible to use this approach for the Roya, where no LiDAR surveys are available before the storm. It is therefore possible that the active channel width of the Roya before the storm has been under-estimated along reaches where the channel was masked by alluvial forest.

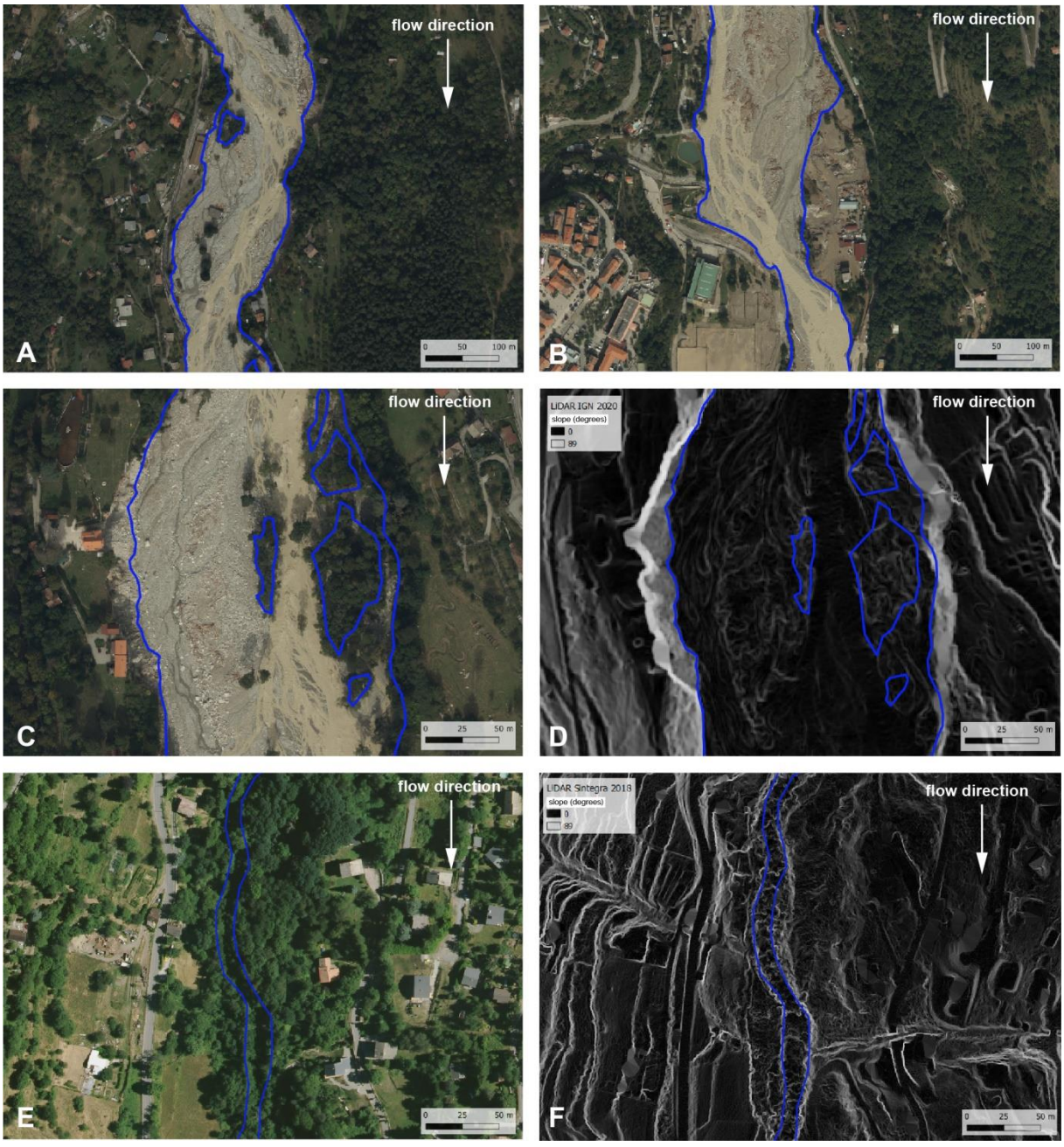

Figure 5. Examples of active channel GIS manual extraction (in blue for every panels): (A) post-Alex active channel extraction in the Boréon valley, showing inclusion of low-flow channels and unvegetated gravel bars, and exclusion of wooded islands; (B) post-Alex active channel extraction of the Vésubie near Roquebillière,

showing exclusion of overbank fine sediment deposition in the left bank; (C and D) post-Alex active channel extraction of the Vésubie near Saint-Martin-Vésubie, illustrating the combined used of ortho-image and LiDAR derived slope raster to exclude an eroded talus on the right bank; (E and F) ante-Alex active channel extraction of the Boréon, illustrating the combined used of ortho-image and LiDAR derived slope raster in a reach where the active channel is masked by riparian vegetation

LiDAR DEMs were also used for the manual extraction of the modern valley floor, defined here as the spatial extent of historical alluvial deposits. This can be seen as the channel shifting space of the last two centuries. In the European Alpine context, those deposits are generally composed of the present-day forested floodplain and the low alluvial terrace of the Little Ice Age (LIA), which is often occupied by softwood forest stands (Bravard, 1989; Liébault and Piégay, 2002; Comiti, 2012). Old terraces from Pleistocene cold periods and alluvial fans from headwater catchments were not included in the modern valley floor. A threshold of 10 m was considered for excluding old terraces; this means that any mainstem fluvial deposit with a relative elevation of less than 10 m with respect to the mean elevation of the active channel was considered as part of the modern valley floor. This is the rule adopted for the valley bottom mapping in the Rhône basin and its Mediterranean margin (Alber and Piégay, 2011). Our own checking of this relative elevation threshold in the Roya and Vésubie valleys, that are part of the Mediterranean margin of the Rhône basin, confirms its efficiency for separating the modern valley floor from Quaternary terraces indicated in the geological maps. Because alluvial fans and old terraces were strongly eroded during Storm Alex, it was necessary to extract the modern valley floor before and after the storm, using the two available LiDAR DEMs. For the Roya, only the post-storm valley floor was extracted. One example of modern valley floor mapping is provided in Figure 6.

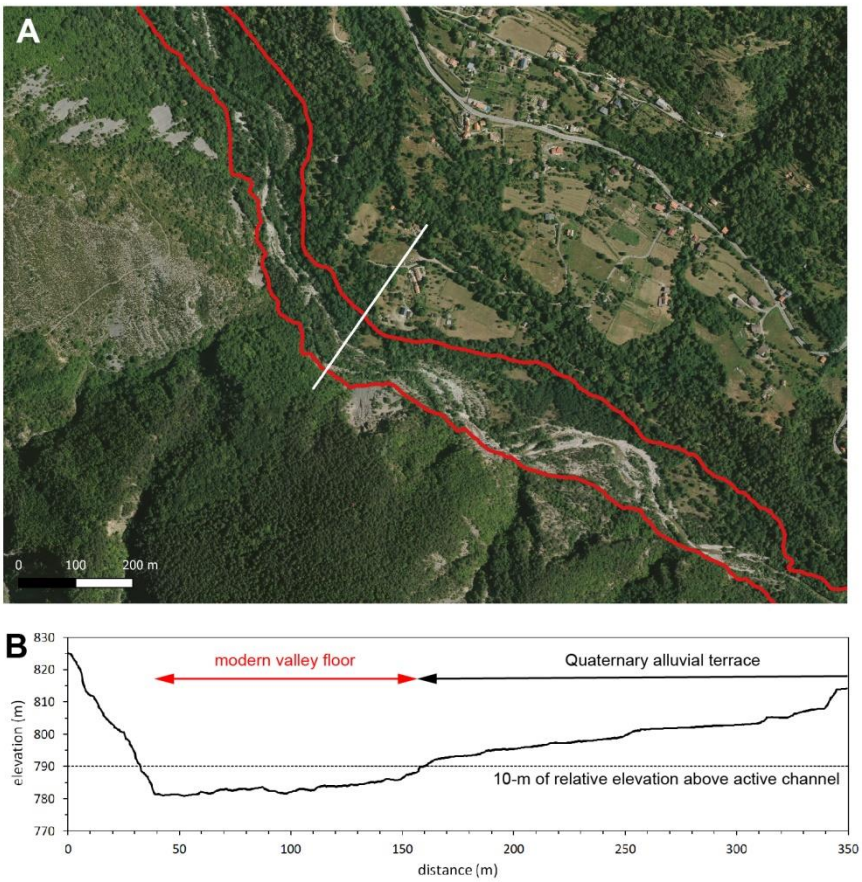

Figure 6. Example of modern valley floor manual extraction in the Vésubie valley obtained from the 2018 LiDAR DEM: (A) extent of the valley floor in red, with localization of the cross-section (in white) shown in panel B; (B) cross-section extracted from the 2018 LiDAR DEM, showing the 10-m threshold of relative elevation above the active channel used for excluding old alluvial terraces

3.3. GIS-based spatial segmentation

A GIS-based spatial segmentation procedure was implemented to extract active channel width distributions for every investigated dates and to explore longitudinal patterns of 2D morphological adjustments following Storm Alex. The segmentation is based on a suite of GIS processing steps based on the QGIS plugin *Geometric Attributes* (Nyberg et al., 2015) and QGIS SAGA toolbox (Fig. 7). The post-Alex modern valley floor was used as the common spatial reference for segmentation. The centerline extraction of this spatial unit and the automatic positioning of perpendicular transects from the centerline at a regular sampling distance of 100 m allow the segmentation of elementary spatial units. This operation was replicated for all the active channels shapefiles, providing for each

elementary spatial unit the area of the active channel (A) and the length of the active channel centerline (L). The mean active channel width (W) for each spatial unit was obtained by $W=A/L$.

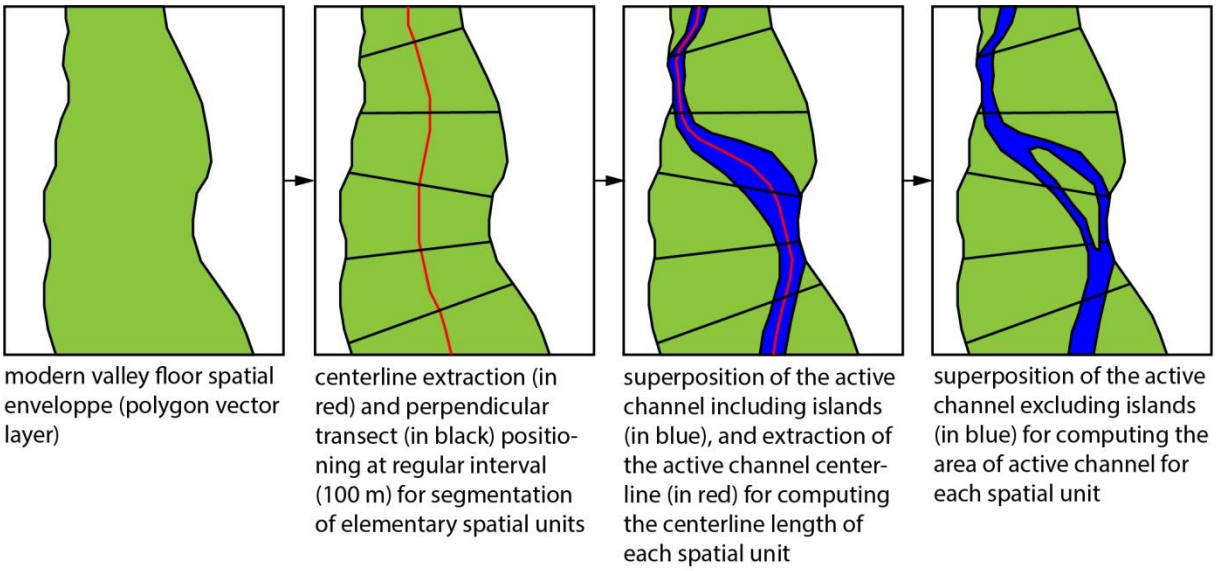

Figure 7. General principle of the GIS spatial segmentation procedure implemented with QGIS plugins for the computation of active channel width

3.4. Sediment budget analysis and bed-level changes

Airborne LiDAR surveys of November 2018 and October 2020 were used to compute a sediment budget of Storm Alex along the study reaches of the Vésubie River basin, and along the most active tributaries. This analysis being based on infrared LiDAR, it does not take bathymetry into account. However, the low proportion of water surfaces in the post-flood active channel and the magnitude of topographic changes observed after the storm lead to think that this limitation should have a low effect on computed erosion and deposition volumes. A co-registration of 3D point clouds was done with CloudCompare (https://www.danielgm.net/cc/) to reduce as much as possible the systematic error of topographic differencing, as recommended by several authors (e.g. Lallias-Tacon et al., 2014; Anderson, 2019). A local co-registration was done by considering tiles of 1 km length and 500 m width. A first set of stable zones in the vicinity of the river channel was selected for calibrating the transformation matrix of each tile, and a second independent set was used to compute the mean error of elevation in stable zones (ME), which is equivalent to the residual systematic error after co-

registration ($ME=\frac{1}{n}\sum(Z_{2020}-Z_{2018})$, with Z_{2020} the elevation from the 2020 LiDAR survey, and Z_{2018} the elevation from the 2018 LiDAR survey). This pre-processing step allowed reducing the systematic error of elevation from 16 cm to -1.1 cm in the lower Vésubie, from 7.5 cm to -0.16 cm in the upper Vésubie, from 4.9 cm to -0.8 cm in the Boréon, and from 8.9 cm to 0.8 cm in tributaries.

Erosion and deposition volumes were computed with the QGIS raster analysis toolbox using the DEM of Difference (DoD) obtained by subtracting the two co-registered LiDAR surveys. An area of interest was manually delimited along the study reaches to restrict the volume computation to erosion and deposition induced by fluvial processes along mainstems. This area is composed of the post-Alex active channel, vegetated islands of the floodplain, and active margins of the active channel (Fig. 8). Active margins can be easily detected from the post-Alex DoD; they correspond to sediment deposition zones of the floodplain, and lateral sediment recruitment zones from remobilization of alluvial terraces, alluvial fans, and footslopes. Sediment erosion and deposition volumes along selected tributaries were also extracted inside a mask manually delimited along the stream network and its active margins, including all the active connected hillslope sediment sources visually detected from topographic differencing. This analysis was conducted on 35 tributaries that have been considered as significant sediment suppliers to the mainstem according to geomorphic activity detected on alluvial fans by topographic differencing (Fig. 9). Geomorphic activity was considered as significant when widespread erosion and deposition zones are detected in the DoD. Tributaries of the upper Boréon valley (upstream from the upper end of the Boréon study reach) were not considered in the analysis because a major reservoir dam has efficiently trapped sediment transport from this part of the catchment, as attested by the incomplete filling of the reservoir during Storm Alex. In few tributaries (n=7), catchments were partially covered by the October 2020 LiDAR survey, so topographic differencing of uncovered surfaces was obtained with a 2021 LiDAR survey from IGN. Only unclassified raw LiDAR point clouds were available for this survey, so an automatic extraction of ground points was done with R using the lidR package (Roussel et al., 2020), and classification errors were manually corrected with CloudCompare. This procedure gives DEMs of good quality,

except for the Venanson catchment, where a low ground point density was obtained due to a dense forest cover. Results from topographic differencing for this catchment must then be considered with caution.

Gross erosion and deposition volumes were computed after a DoD thresholding, considering a spatially uniform level of detection (*LoD*) equal to 0.13 cm. This value was obtained from root mean square errors (*RMSE*) of LiDAR elevations computed for the 2018 and 2020 surveys, using a set of 128 ground control points measured with a dGPS in stable areas by the private company in charge of the 2018 survey. The *LoD* was computed using a 95% confidence interval ($LoD = 1.96(RMSE_{2018}^2+RMSE_{2020}^2)^{0.5}$) (Lane *et al*., 2003). Approaches based on a spatially distributed error were not considered here, since they have been mostly developed for improving change detection of areas experiencing a small morphological activity (Wheaton et al., 2010; Milan et al., 2011). After thresholding, the *LoD* was subtracted from all DoD cells for the computation of gross erosion and deposition volumes, following recommendations from Carley *et al*. (2012). Thresholding of the DoD was not considered for the net sediment budget computation, as thresholding can be a source of bias and error in net change analysis (Lane et al., 2003; Anderson, 2019). Uncertainty bounds of sediment volumes were computed following the procedure presented by Anderson (2019), using the following equation:

$$\sigma_v = nL^2\sqrt{\frac{\sigma_{rms}^2}{n}+\frac{\sigma_{sc}^2}{n}\frac{\pi a^2}{5L^2}+\sigma_{sys}^2} \qquad (1)$$

with σ_v the volume uncertainty (m^3), n the number of DoD cells in the analysis, L the cell size (m), σ_{rms} the uncorrelated random error (m), computed here as $\sigma_{rms} = (RMSE_{2018}^2+RMSE_{2020}^2)^{0.5}$, σ_{sc} the spatially correlated random error (m), πa^2 the circular area over which errors are correlated (m^2), and σ_{sys} the systematic error, which was considered here as equal to the residual systematic error after co-registration. The spatially correlated random error and the πa^2 term were obtained from a semi-variogram analysis performed using the ArcGIS kriging tool, following the procedure described in Anderson (2019).

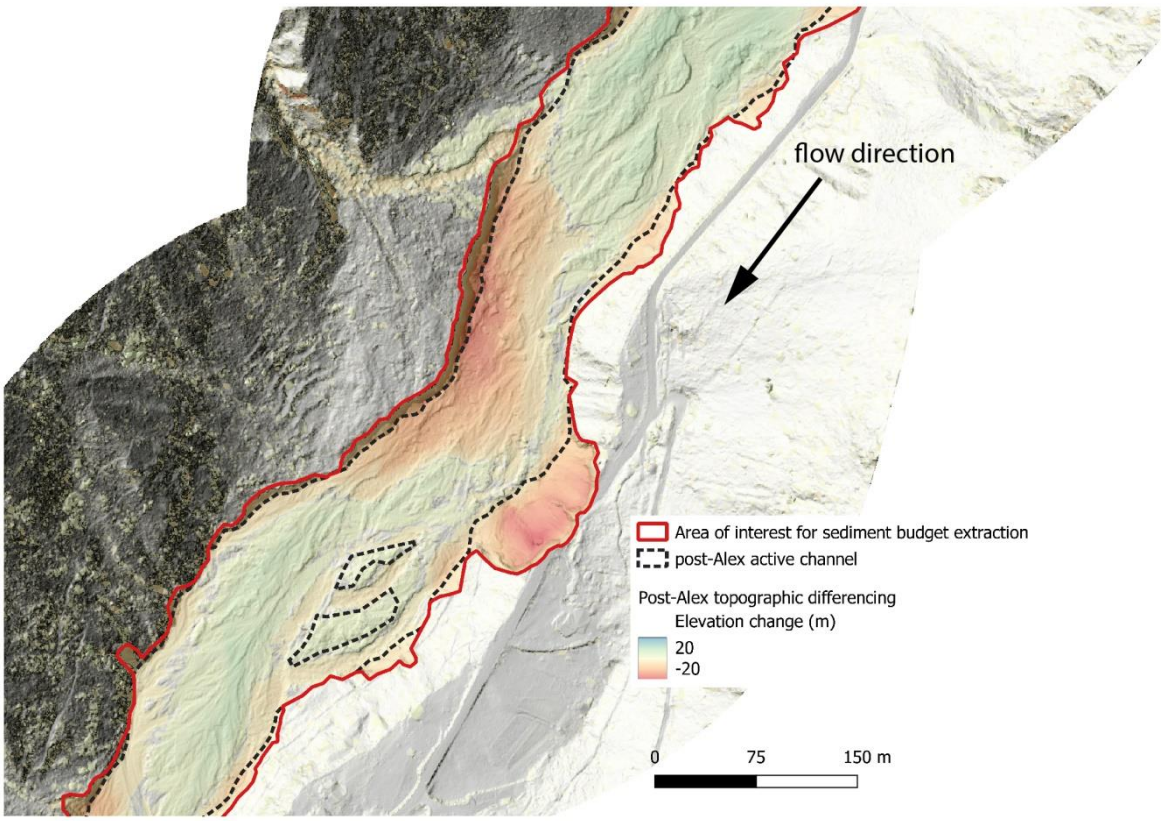

409

410 Figure 8. Example of area of interest used for extracting post-Alex erosion and deposition volumes along
411 mainstems; this area is not limited to the post-Alex active channel, as it also includes active parts of the valley
412 floor which can be easily detected from the post-Alex DoD; in this example, lateral sediment supply from bank
413 erosion of an alluvial fan on the right bank, and of an old alluvial terrace on the left bank, are clearly visible;
414 background: hillshade view of the 2020 LiDAR DEM

415

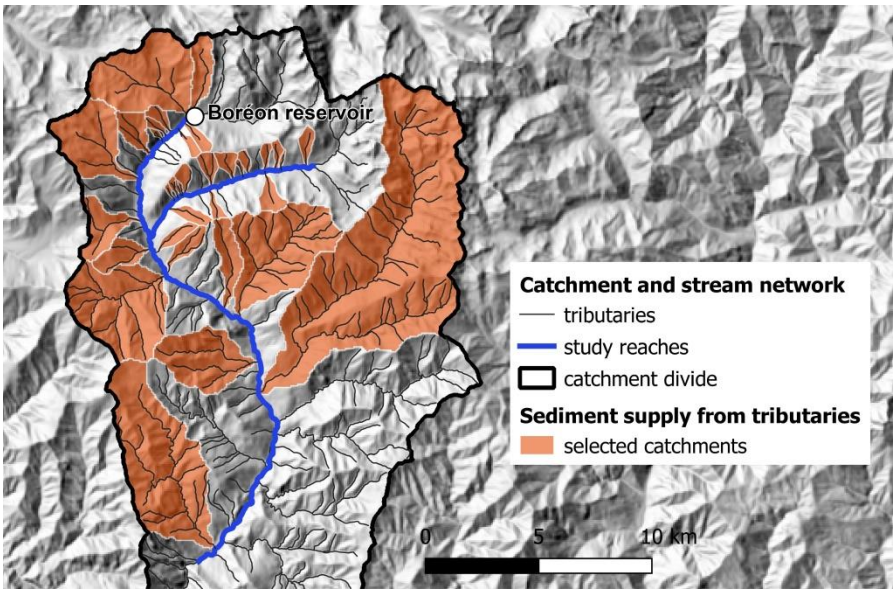

416

Figure 9. Map of selected tributary catchments of the Vésubie for sediment supply assessment with LiDAR-based topographic differencing data

Sequential LiDAR surveys were also used to reconstruct post-Alex bed-level changes along the study reaches of the Vésubie catchment. The zonal statistics QGIS plugin was used to extract ante- and post-Alex mean active channel elevations (excluding bathymetry) for each segmented spatial unit (see section 3.3). Ante-Alex active channel elevation was extracted from the co-registered 2018 LiDAR survey and the 2017 active channel layer. Post-Alex active channel elevation was extracted from the co-registered 2020 LiDAR survey and the 2020 active channel layer. By comparing mean active channel elevations before and after the storm, it was possible to explore the longitudinal pattern of bed-level changes and to look at cross-correlations with 2D morphological adjustments.

4. Results

4.1. Active channel responses

Ortho-images taken before and after Storm Alex show that the active channel surface of the Vésubie has increased by a factor 4 after the storm; from 68 ha in 2017 to 274 ha in 2020 (Fig. 10). This active channel expansion is far greater than the surface increase attributable to the November 1997 flood, which has been estimated at only 21 ha (from 94 ha in 1995 to 115 ha in 1999). The mean active channel width increased from 19 m to 79 m after the storm, and from 27 m to 33 m after the 1997 flood (Fig. 11A). The 2D morphological effect of Storm Alex is therefore 10 times greater than that of the last 100-yr flood in the valley. Archives of aerial imagery clearly reveal the exceptional nature of this geomorphic impact for the last 70 years, the mean active channel width of the Vésubie having stayed below ~30 m since at least 1948 (Fig. 11A). The singular geomorphic signature of the storm is also illustrated by the expansion of the modern valley floor, which has increased form 317 ha in 2018 to 363 ha in 2020, under the effect of lateral erosion of colluvial deposits and fluvio-glacial terraces. Almost all of the post-Alex modern valley floor has been occupied by the new active channel (76%); this channel confinement index has never exceeded 36% during the last 70 years.

The active channel surface of the Roya increases by a factor 2.3 after the storm; from 59 ha in 2017 to 137 ha in 2020 (Fig. 10). The mean active channel width increased from 15 m to 37 m (Fig. 11B). It was not possible to make a comparison with precedent extreme floods for the Roya, because the last major historical flood occurred in November 1926, before the first set of aerial images. However, like for the Vésubie, the post-Alex geomorphic response of the Roya does not have any antecedent analog during the last 70 yrs. The post-Alex channel confinement index is 75%; this value is equivalent to the Vésubie, and it reflects a similar relative geomorphic resetting of the valley floor. The absence of a LiDAR survey before the event prevented us to map the modern valley floor before the flood, but the very hard bedrock outcrops constituting the limits of the Roya valley floor let us think that the valley floor expansion observed in the Vésubie did not occur in the Roya, or only very occasionally.

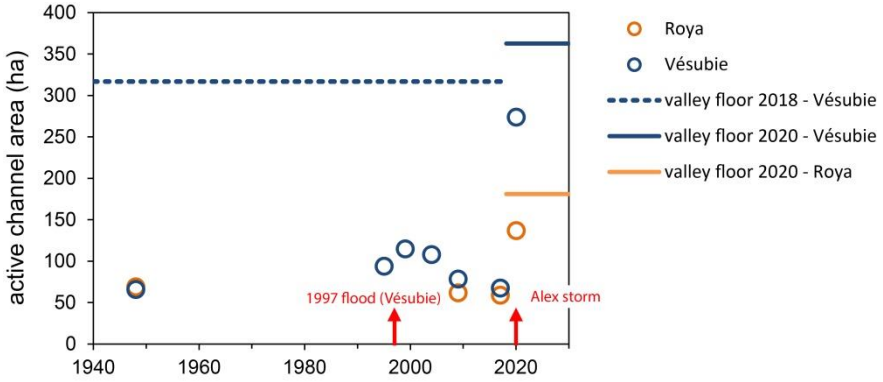

Figure 10. Time evolution of the active channel surface of the Roya and Vésubie rivers; surfaces occupied by modern valley floors give the available space for active channel development in the two valleys

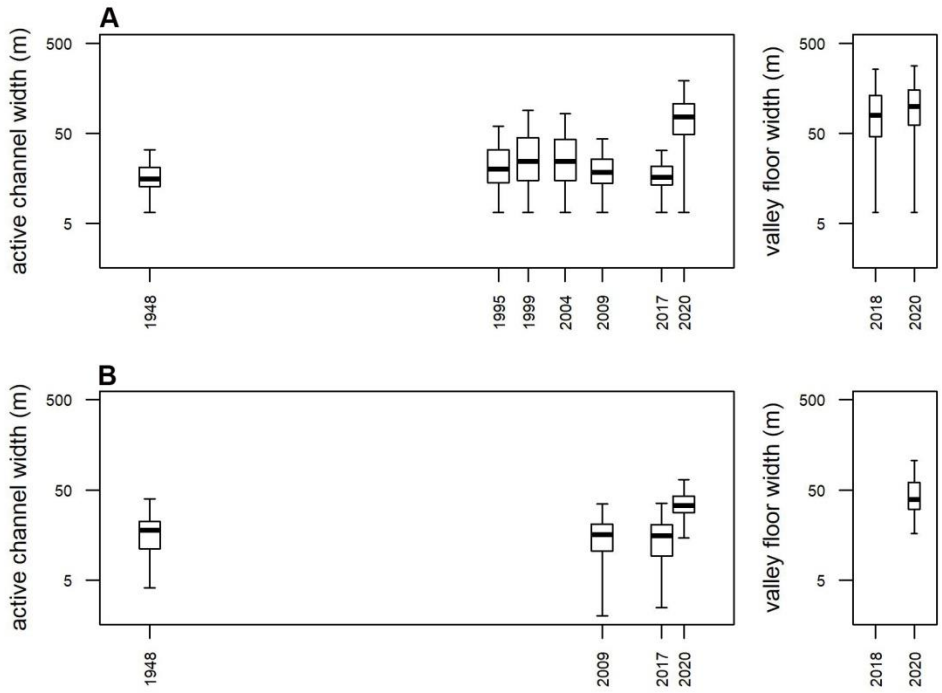

Figure 11. Box plots of active channel width distributions at different dates, compared with valley floor width distributions for the Vésubie (A) and Roya (B)

4.2. Longitudinal patterns of 2D morphological changes

The longitudinal gradient of the geomorphic response to Storm Alex for the Vésubie shows a quasi-continuous active channel expansion along the 35 km study reach (Fig. 12A). The single-thread pattern with local wandering or braiding spots that prevailed along this reach since the late 1940s has been replaced by a wide multi-thread braided pattern almost everywhere. The only stable portions of the valley correspond to the two narrow gorges located downstream of Lantosque. Braided channel formation has been observed wherever space was available in the valley floor. A major limitation of active channel expansion by hillslopes and Pleistocene fluvio-glacial terraces is observed in upper valleys, even if those have been locally eroded as attested by the increase of the modern valley floor width. It is not really the case anymore in the lower half of the study reach, where many local channel expansions have not been laterally constrained by the valley floor boundaries. Although active channel expansion of the Roya is also observed along almost all the 36 km study reach, a different longitudinal pattern appears, with more pronounced lateral controls of channel expansion downstream than upstream (Fig. 12B). This is partly related to the distribution of narrow proglacial gorges which are

more developed in the lower part of the study reach. Contrary to the Vésubie, braided channel formation was only marginally observed in the upper part of the valley, upstream of the confluence with the Réfrei. The dominant channel pattern that get formed after the storm in the alluvial parts of the valley is a wandering pattern.

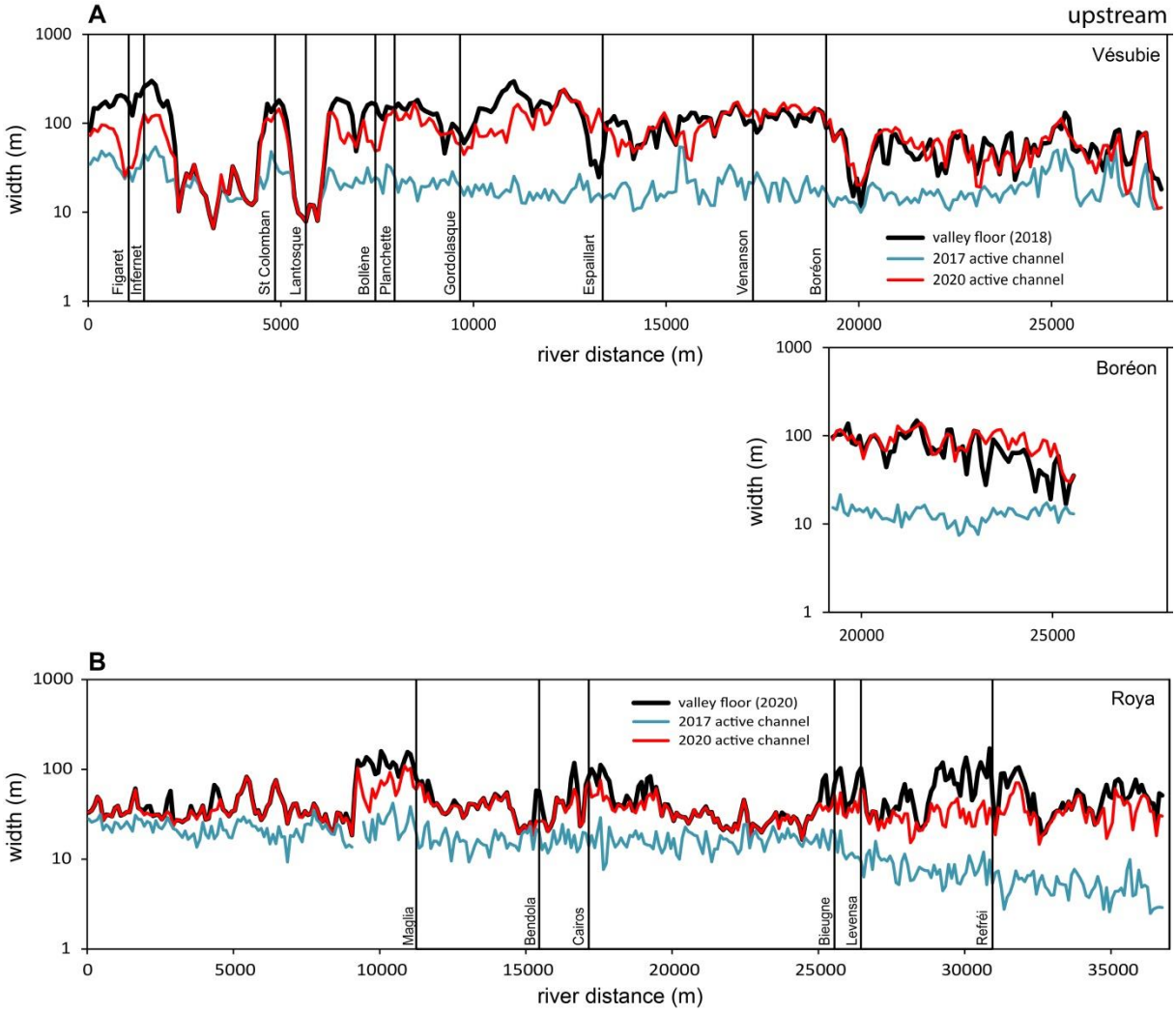

Figure 12. Longitudinal gradients of post-Alex active channel expansion in the Vésubie (A) and Roya (B) study reaches; vertical lines correspond to major tributary confluences

The index of confinement (*IC*, computed as the ratio between post-Alex active channel width and modern valley floor width) can be used to visualize spatial patterns of active channel expansion relative to a local maximum potential expansion. If alluvial portions of the valley are considered, based on a threshold separating alluvial and gorges reaches (see supplementary material), a downstream decrease of this index is observed for the Vésubie (Fig. 13), with a first decreasing step at

a river distance of around 16 km, and a sharp decline downstream the last gorges. This cannot be attributed to an increase of the valley floor width, which fluctuates around a constant mean of ~130 m in the lower 13 km of the study reach, excluding gorges sections (Fig. 12). The Roya does not show any clear longitudinal pattern. A more chaotic signal is observed for this river, each alluvial cell of the valley floor (defined as alluvial units comprised between gorges) showing a specific response.

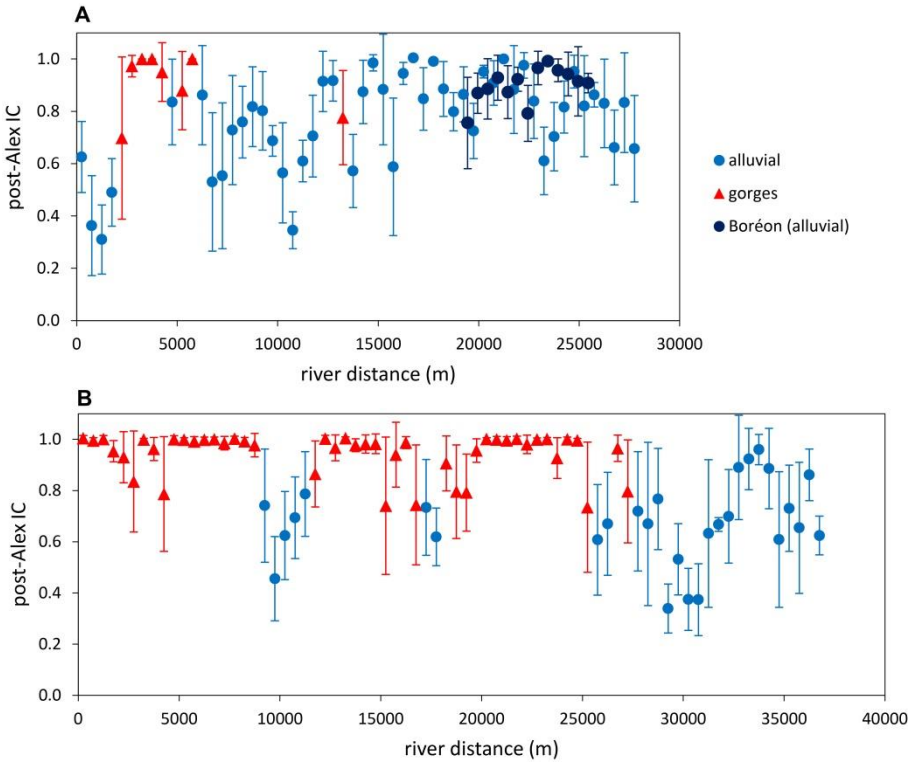

Figure 13. Longitudinal gradients of the post-Alex index of confinement (*IC*) for the Vésubie (A) and Roya (B); the index of confinement corresponds to the ratio between post-Alex active channel width and modern valley floor width; data points correspond to mean values computed for 500 m intervals; error bars correspond to ± one standard deviation; points were classified as gorges or alluvial units according to a scaling law of valley floor width vs. drainage area obtained for the Vésubie (see supplementary material)

The width ratio, obtained by considering the ratio between post-event and pre-event active channel widths, is classically used to characterize the flood impact on channel widening. Longitudinal gradients of width ratio for the two rivers show very different patterns (Fig. 14). In the case of the Vésubie, the higher widening rates are observed in the middle part of the study reach, and a regular downstream decrease is observed from a river distance of around 11 km. Once again, a sharp decline is

observed downstream the last gorges. The Roya is characterized by a regular downstream decrease of the width ratio up to a river distance of 25 km. From this point, the widening rate stays at a low level down to the lower end of the study reach.

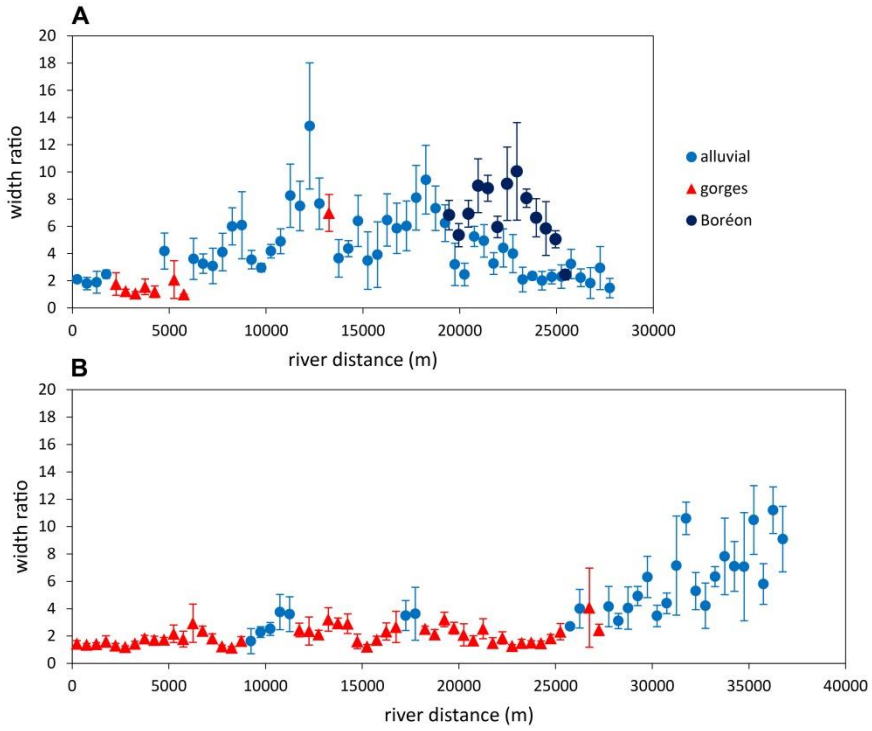

Figure 14. Longitudinal gradients of the Storm Alex width ratio for the Vésubie (A) and Roya (B); data points correspond to mean values computed for 500 m intervals; error bars correspond to ± one standard deviation; points were classified as gorges or alluvial units according to a a scaling law of valley floor width vs. drainage area obtained for the Vésubie (see supplementary material)

4.3. Bed-level changes

Active channel altimetric changes obtained from LiDAR-based topographic differencing show a quasi-continuous channel aggradation of the Vésubie after Storm Alex, with local values exceeding 10 m in upper valleys (Fig. 15). The mean value for the study reach is 2.4 m, with a range comprised between -3.2 m and 11.2 m. Hot spots of aggradation are located in the Boréon and in the middle part of the Vésubie valley, near the confluence with the Boréon and downstream of the confluence with the Espaillart. This tributary joins the Vésubie just downstream of a major nickpoint in the long profile, with a local increase of slope, where channel incision has been observed during the storm. The longitudinal pattern of aggradation magnitudes shows some similarities with that of the channel

confinement index and width ratio (Fig. 13 and 14), with a first decreasing step at a river distance of 12 km, and another one downstream of the last gorges. Some local incisions are observed in the upper valleys, and in downstream gorges.

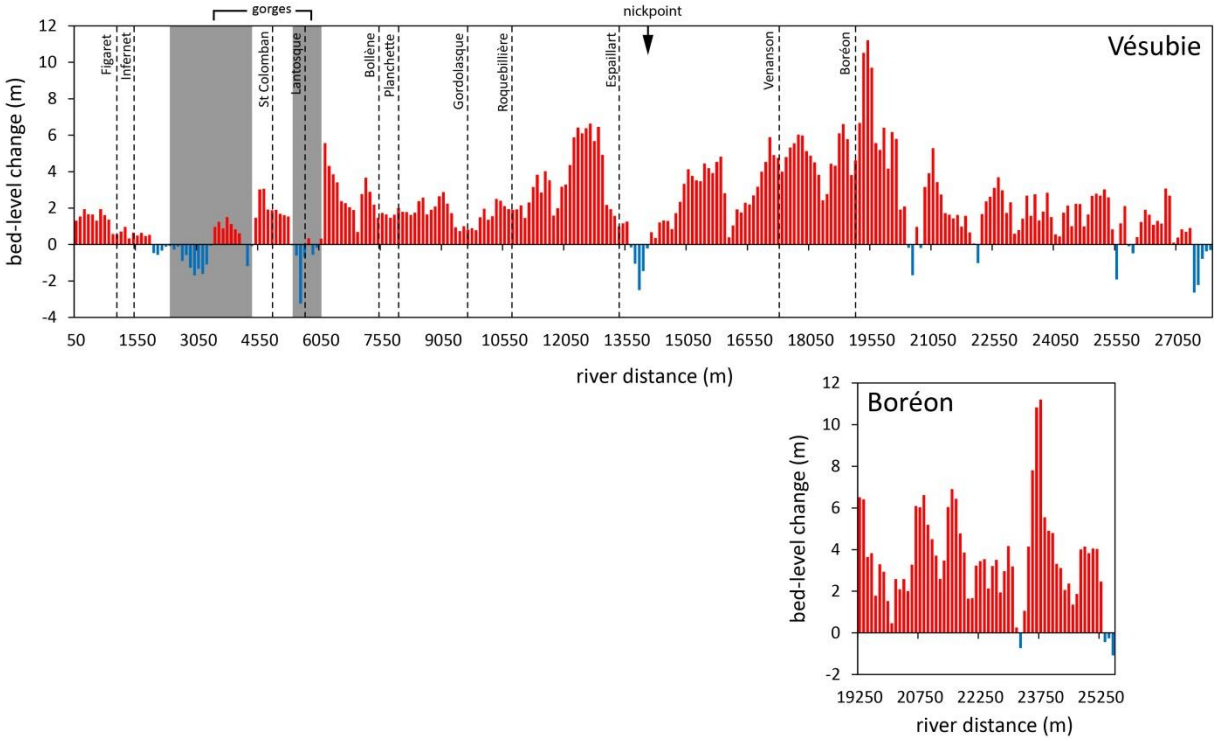

Figure 15. Bed-level changes of the Vésubie after Storm Alex obtained from topographic differencing of LiDAR DEMs; aggradation in red and incision in blue; vertical dotted lines correspond to main tributary confluences; gorges are represented in grey; the back arrow corresponds to a major nickpoint in the long profile, with a local slope increase

4.4. Controls on width ratios

Width ratios obtained for the Roya (mean = 3.26, standard deviation = 2.53, maximum = 13.9) and Vésubie (mean = 4.65, standard deviation = 2.94, maximum = 19.0) are among the highest reported values for extreme floods of European mountain rivers and streams (Tab. S1).Width ratios of Storm Alex first confirm a negative correlation with the initial channel width, as previously reported by several case studies addressing geomorphic responses to major floods in temperate mountain environments (Fig. 16). Roya data points are relatively well aligned with the compiled scatterplot, but

542 those from the Vésubie are clearly plotting as an upper envelope, indicating significantly higher
543 widening rates for a given initial width.
544

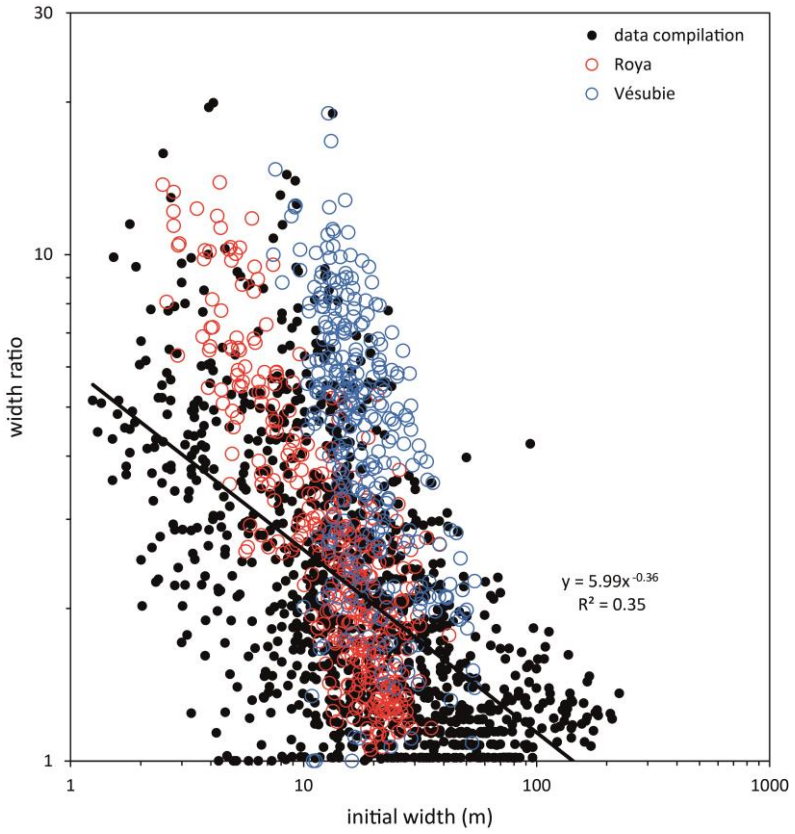

545

546 Figure 16. Width ratios of Storm Alex as a function of the pre-flood active channel width for the Roya and
547 Vésubie, compared to reported width ratios in temperate upland environments (data from Arnaud-Fassetta et al.,
548 2004; Krapesch et al., 2011; Rinaldi et al., 2016; Surian et al., 2016; Righini et al., 2017; Ruiz-Villanueva et al.,
549 2018; Scorpio et al., 2018; Scorpio et al., 2022; Brenna et al., 2023) (see Tab. S1, supplementary material); the
550 best fit was computed for the compiled dataset only
551

552 Several potential predictors of width ratios were tested using the Vésubie dataset only, since
553 information is missing for the computation of these predictors in the Roya. The first tested predictor is
554 a proxy of hydraulic forcing. As previously mentioned, gauging stations of both rivers were destroyed
555 during the storm, consequently no measured peak discharges could be used to calculate the stream
556 power on both rivers. However, it has been possible to compute a stream power index (*SPI*) :

557 $$SPI = \frac{A_d \cdot s}{w_{pre}} \qquad (2)$$

with A_d the drainage area (km²), s the channel slope before the flood (m m^{-1}), and w_{pre} the active channel width before the flood (m). This simple index implies a peak discharge linearly proportional to the drainage area, and does not consider rainfall distributions that clearly show an upstream concentration of high-intensity rainfall cells (Fig. 3). Consequently, this proxy is smoothing the actual spatial variability of the stream power that was most probably higher in the upstream reaches. However, if alluvial reaches are considered, a significant positive non-linear relation was obtained with the width ratios ($wr = 11.53\ SPI^{0.62}$, with wr the width ratio, R^2=0.40, p<0.0001) (Fig. 17A). The effect of valley confinement was also tested by considering the index of confinement before the storm ($IC = w_{pre}/w_{vf}$, with w_{vf} the modern valley floor width before the storm). A significant negative non-linear relation was obtained by considering together stream reaches classified as alluvial and gorges ($wr = 1.27\ IC^{-0.77}$, R^2=0.59, p<0.0001) (Fig. 17B). Width ratios were also cross-compared with bed-level changes of the active channel (Fig. 17C). This comparison shows a positive linear correlation by considering together stream reaches classified as alluvial and gorges ($wr = 0.72\Delta_z + 2.94$, R^2=0.30, p<0.001, with Δ_z the bed-level change). Despite a strong data scattering, it clearly appears that the rate of active channel expansion is partly controlled by the magnitude of net sediment accumulation at reach scale.

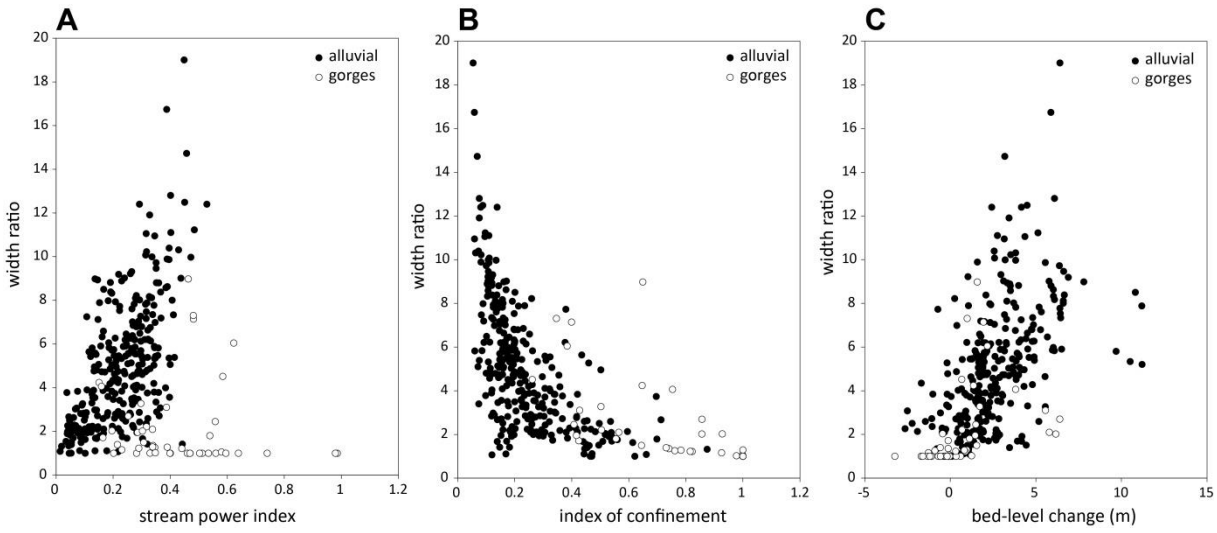

Figure 17. Width ratio of the Vésubie and Boréon channels during Storm Alex as a function of the stream power index (A), the index of confinement before the flood (B), and bed-level change of the active channel during the flood (C).

579 4.5. Alex storm sediment budget for the Vésubie

580 Topographic differencing using LiDAR data collected before and after Storm Alex along the 35 km
581 study reach of the Vésubie catchment allows estimating a total sediment erosion of 4.13 Mm^3 ± 11 000
582 m^3 (mean unit erosion rate in the area of interest of 1.27 m^3 m^{-2}), and a total sediment deposition of
583 3.49 Mm^3 ± 16 000 m^3 (mean unit deposition rate in the area of interest of 0.83 m^3 m^{-2}) (Fig. 18). The
584 cumulative sediment supply from tributaries is estimated at 1.51 Mm^3 ± 25 600 m^3 (Fig. 18, Table S2).
585 The net sediment budget shows 2.06 Mm^3 of sediment yield at the exit of the study reach (± 50 000
586 m^3). This value must not be considered as bed material yield, since it certainly incorporates an
587 important fraction of fine sediments that has been transported in suspension during the flood.
588
589 The cumulative sediment transport along the three study reaches clearly shows a rapid downstream
590 increase of sediment transport in the two upper valleys, under the cumulative effect of sediment supply
591 from local erosion and tributaries (Fig. 19). A decrease of sediment transport is observed downstream
592 of the Boréon-Upper Vésubie confluence, due to a positive net sediment budget in the valley floor and
593 a low supply from tributaries, but this short buffering zone is rapidly interrupted downstream of the
594 confluence with the Venanson (river distance of 17 250 m), where sediment transport increases again
595 under the effect of local erosion and tributary inputs down to the exit of the study reach. Sediment
596 supply from local erosion largely exceeds that from tributaries along the three study reaches. The most
597 active zones of sediment recruitment from local erosion are the upper valleys and the reach of the
598 Vésubie located downstream of the long-profile nickpoint (Fig. 17), where local channel incision has
599 been observed (Fig. 15).

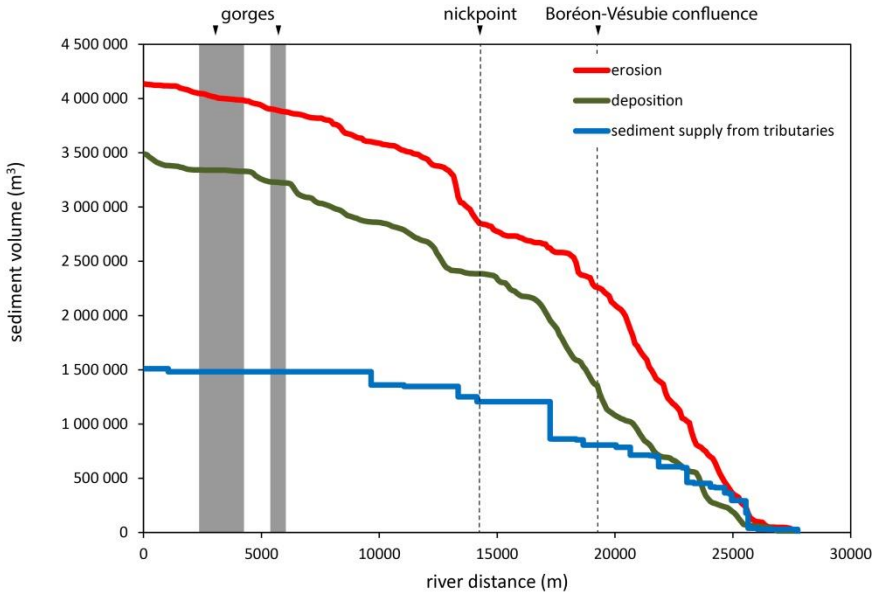

600

601 Figure 18. Cumulative volumes of sediment erosion and deposition in main stem valley floors, and cumulative
602 sediment supply from tributaries obtained from LiDAR-based topographic differencing in the Vésubie catchment
603 during Storm Alex; uncertainty bounds of sediment volumes are included in the thickness of lines

604

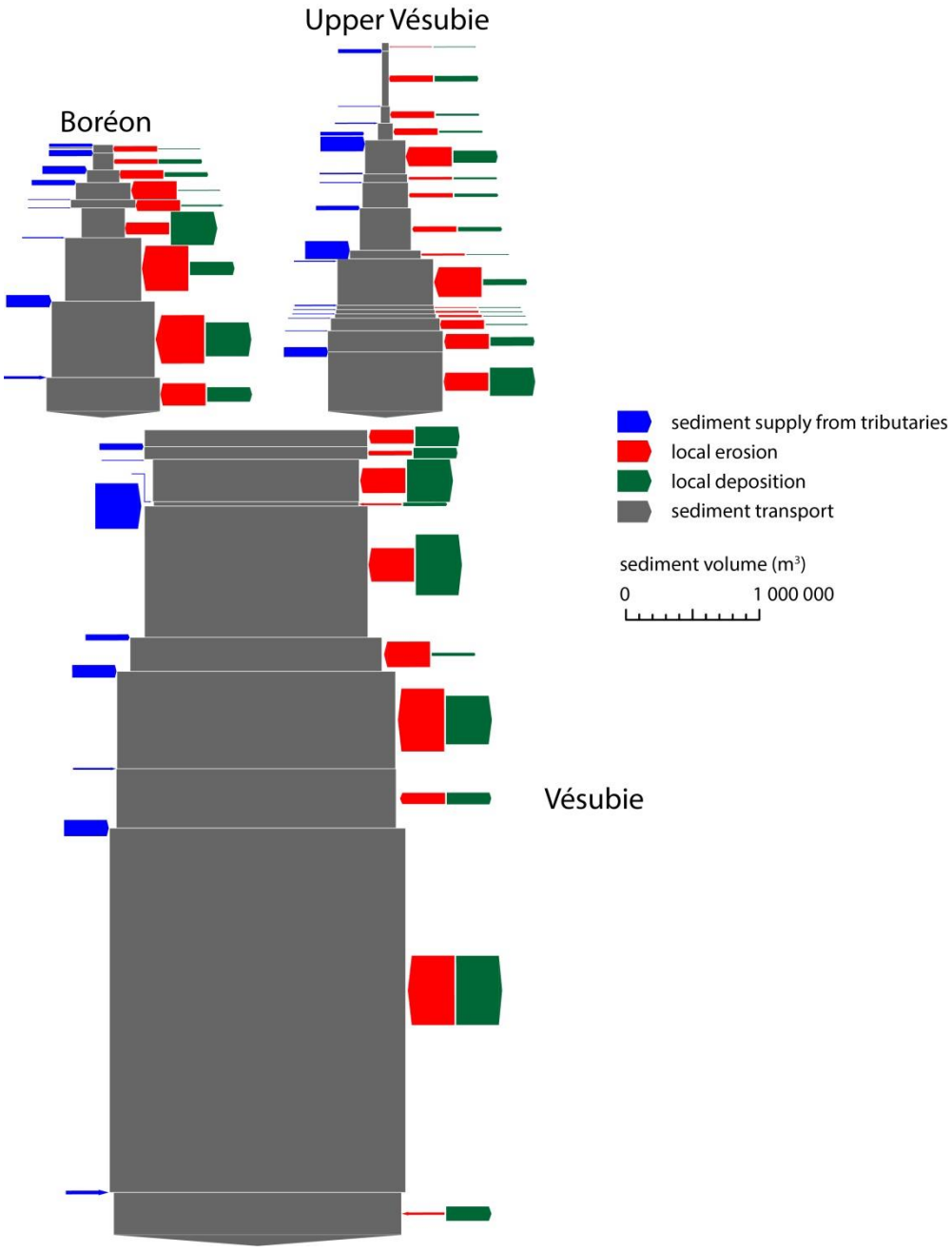

Figure 19. Sediment transport along the three study reaches of the Vésubie catchment during Storm Alex, with sediment supply from tributaries, and local sediment erosion and deposition from the valley floor. Widths of arrows are proportional to sediment volumes. Heights of grey segments for the 3 sub-reaches (Boréon, Upper Vésubie and Vésubie) are proportional to their lengths. Grey segments are delimited between tributary inputs.

5. Discussion

5.1. Storm Alex impact in the historical trajectory of the rivers

613 Reconstructions of channel responses to Storm Alex in the Vésubie and Roya valleys reveal major
614 geomorphic impacts with no antecedent analogs during, at least, the last 70 years for both rivers, as
615 attested by historical active channel changes (Fig. 9 and 10). A quasi-continuous fluvial
616 metamorphosis is observed along the investigated stream networks, from single-thread to braiding in
617 the Vésubie, and from single-thread to wandering in the Roya. Although some braided patterns
618 emerged locally in the upper Roya, the dominant physical configuration in narrow proglacial gorges
619 strongly limited braided channel formation in this valley. The physical setting is quite different in the
620 Vésubie, a glaciated valley during the Last Glacial Maximum, where alluvial landforms related to
621 glacial imprints are much more present. It is remarkable to see that braided channel formation during
622 the storm is spatially coincident with the formerly glaciated portion of the Vésubie valley. Fluvio-
623 glacial outwash plains that set up during the last glacial recession phases are at the origin of the
624 formation of the relatively wide alluvial plains prone to braiding development. The different glacial
625 imprints between the two valleys can therefore be considered as a key factor explaining the contrasted
626 geomorphic responses of both rivers.
627
628 Storm Alex induced dramatic active channel widening along almost all the investigated stream
629 networks of the Vésubie and Roya. In the Vésubie, the active channel widening is associated with a
630 strong aggradation (Figure 17C). These are typical morphological adjustments related to extreme
631 floods under conditions of very high sediment supply (e.g. Arnaud-Fassetta et al., 2005; Rinaldi et al.,
632 2016). However, what is really exceptional is the magnitude with which those adjustments occur,
633 notably in the Vésubie. The comparison in the Vésubie between Storm Alex and the last noticeable
634 flood of 1997 (return period estimated at about 100-yrs for the upper catchment) shows an order of
635 magnitude difference in terms of active channel expansion. This dramatic intensity of channel
636 widening is in good agreement with estimated return periods of hydro-meteorological forcings, largely
637 exceeding 100 years. Similar flood-induced values of channel widening after catastrophic floods are
638 generally found in streams with much smaller catchment-size than the Vésubie (Table S1). The only
639 reported case of mean channel widening equivalent to the Vésubie (width ratio of 4.6) for a catchment-
640 size of several hundreds of km² is the August 2005 flood in the Trisanna River of the Austrian Alps,

with a mean width ratio of 4.1 (Krapesch et al., 2011). The estimated return period of rainfall forcings of this event (≥ 1000 yrs) is also similar to Storm Alex. The mean width ratio for the June 1957 flood in the Guil, which can be viewed as the last analog of Storm Alex in terms of geomorphic response in the French Alps, is only 2.3 (Arnaud-Fassetta and Fort, 2004).

The documentation of channel aggradation in the Vésubie also provides some exceptional values, with a maximum around 10 m in proximal reaches, and with values exceeding 4 m along reaches of several km in length (Figure 13). These values largely exceed the few reported maximum flood-induced aggradation values in alpine environments, that most often do not exceed 2 m on long distances (Scorpio et al., 2018; Scorpio et al., 2022). Unfortunately, most of the recently reported case studies of extreme floods in alpine environments are restricted to 2D morphological effects, simply because data are generally missing for documenting bed-level changes. One exception is the October 2018 Vaia storm in Northeast Italy (200 yrs return period, Brenna et al., 2021), where topographic differencing from sequential LiDAR surveys has been used to document post-flood erosion and deposition along valley floors of the Tegnas Torrent (Pellegrini et al., 2021) and Rio Cordon (Rainato et al., 2021). Results from the Tegnas case study have shown contrasted bed-level changes, with an alternating sequence of aggradation (maximum values < 4 m) and incision along a 6-km reach. In the Rio Cordon, the dominant channel response was channel incision related to the breaking of the coarse surface layer. To find magnitudes of rapid channel aggradation equivalent to Storm Alex (>5-10 m), it is necessary to look at rivers that have been impacted by catchment-scale deforestation (Marutani et al., 1999; Gomez et al., 2001; Gomez et al., 2003; Liébault et al., 2005) or by sediment waves coming from landslides (Korup, 2004) or debris-flow torrents (Liébault et al., 2013).

The oldest available aerial photographs show that in the relatively wide alluvial plain of the Vésubie valley, the dominant channel morphology of the late 1940s was a single-thread pattern with few active gravel bars. This situation is not very common for alpine gravel-bed rivers of that time, most of them showing much wider active channels than today, with dominant fluvial patterns like braiding or wandering (Bravard, 1989; Liébault and Piégay, 2002; Comiti, 2012; Nardi and Rinaldi, 2015). Wide

669 active channels of the mid-20th century have been interpreted as a legacy from high sediment supply
670 conditions that prevailed during the LIA, under the cumulative effect of more erosive climatic forcings
671 and human-induced deforestation on hillslopes. Most of these wide active channels rapidly
672 transformed into fluvial terraces 1950s onward, due to sediment supply decrease and human pressures
673 (e.g. gravel mining, dams). However, it has been recently shown that extreme floods may recreate
674 active channels as wide as they were in the 1950s (Nardi and Rinaldi, 2015). The historical trajectory
675 of the Vésubie deviates from this narrative (this is also the case of the Roya, but narrow gorges in this
676 valley prevents comparison with other alpine rivers). Active channel evolution of the last 70 years in
677 the Vésubie rather show the permanence of a narrow single-thread channel, with marginal
678 morphological activity. This cannot be attributed to a low hydrological activity, since several large
679 floods occurred during this period, mainly during the 1950s and 1990s (Fig. 4). This means that the
680 Vésubie was adjusted for a long time to a low sediment supply from its catchment before Storm Alex
681 hits. Major sediment sources on hillslopes are limited to 4-5 permanent and active sediment
682 production zones of small headwater catchments located in the Upper Vésubie (Madone de Fenestre)
683 and Boréon valleys, where sediment supply to the mainstem by debris flows can be considered as
684 relatively regular. This persistent low level of geomorphic activity on headwaters is also suggested by
685 the limited spatial extent of RTM State Forests in the catchment (Fig. 1). These zones cover only 6%
686 of the Vésubie catchment, whereas in other catchments of the Southern French Prealps, they can cover
687 around 20% (Liébault et al., 2008). This could be due to a lower past agricultural pressure than in
688 other alpine valleys, related to harsh topographic conditions (e.g. narrow and steep valleys) or specific
689 historical facts, but this needs to be confirmed by a detailed investigation of past land-use conditions.
690 However, it is possible that braided channels were much more developed in some reaches of the
691 Vésubie during the LIA, as attested by some pictures of the late 19th century (Fig. 20). A cycle of
692 channel recovery likely related to a major flood that occurred in October 1882 (Fig. 4), and that was
693 potentially at the origin of the formation of a braided channel, is clearly visible in Figure 20. Thorough
694 investigations of old maps and cadasters from the 19th century could be of great interest for
695 determining if braiding of the Vésubie was continuously developed along the alluvial plain at that
696 time, notably under the effect of successive large floods that occurred during the second half of the

19th century, or if it was only a transient and localized alluvial landform. It could be also interesting to undertake a specific study of past sediment supply conditions in these catchments, with respect to the history of human pressures (land-use changes, torrent-control works), in order to better understand their specific morphological trajectories.

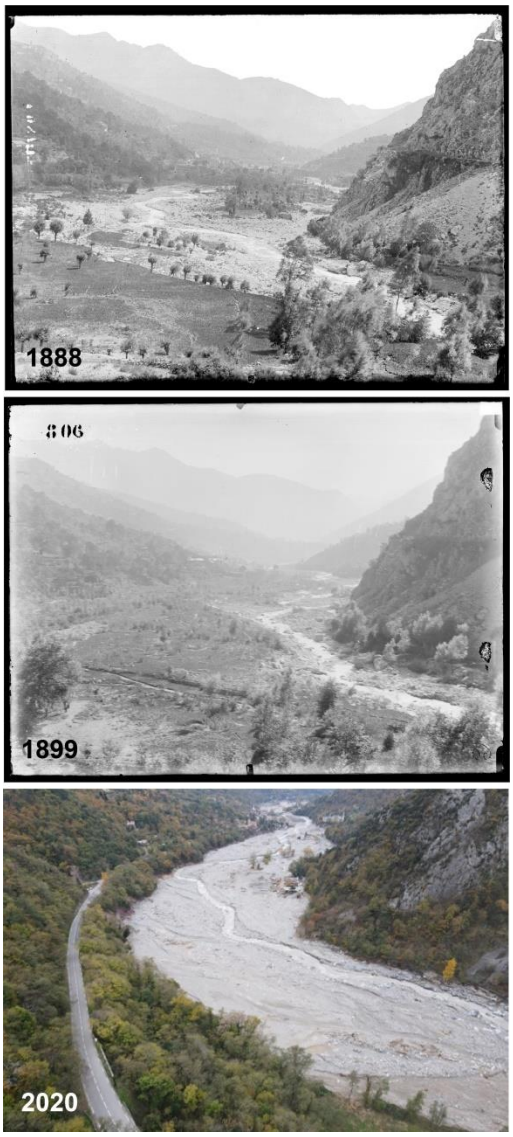

Figure 20. Sequence of pictures of the Vésubie channel in the upstream vicinity of Roquebillière, showing a cycle of channel recovery following a major flood that occurred in October 1882, that was potentially at the origin of the braided channel visible in the 1888 photo (© *Archives Départementales des Alpes-Maritimes, collection Eaux et Forêts, commission des reboisements des Alpes-Maritimes* ; 1888 photo : 23FI 0838; 1899 photo : 23FI 0874). The picture of 2020, taken just after Storm Alex, shows the reformation of a braided channel in this area (© Vincent Koulinski).

The fate of post-Alex braided or wandering channels should theoretically be a rapid recovery, with downstream progressing channel narrowing and incision, and subsequent formation of fluvial terraces, like reported by many case studies of channel recovery after sediment wave propagation (James, 1991; Pitlick, 1993; James, 2010). It is indeed hard to imagine that Storm Alex will initiate a long-term trajectory of active channel widening and aggradation, because the storm did not generated any major destabilization of hillslopes that could persistently sustain a high sediment supply during usual rainfall events, and most of the historical channel shifting space in the valley floor is already occupied by the active channel (76 %). The regime of low sediment supply from hillslopes that prevailed before the storm will likely be restored during the next decades. Channels should therefore relatively rapidly recover a morphology adjusted to this regular regime, unless an increase of flood magnitude and frequency would occur under the effect of climate change. Although recent regional studies have shown a substantial increasing trend of extreme autumn rainfall events in the Southwestern Alps since the late 1950s (Blanchet et al., 2021a), under the effect of increasing Mediterranean circulations (Blanchet et al., 2021b), statistical analysis of flood discharge series in French Mediterranean rivers has revealed that there is no general tendency towards more severe floods in this region (Tramblay et al., 2019). This is in good agreement with detections of flood-rich and flood-poor periods across Europe for the 1960-2010 period, showing a decrease of the frequency of stations with flood-rich periods for the Mediterranean region (Lun et al., 2020). Inverse trends of flood hydrology and extreme rainfall in this region has been interpreted as a consequence of a decreasing soil moisture (Tramblay et al., 2019). All these elements suggest that future trends in hydro-meteorological forcings of channel recovery for the Vésubie and Roya valleys remain quite uncertain.

However, if a downstream progressing channel incision occurs, it will fuel a high sediment supply to distal reaches, and those reaches will need more time to recover. The “legacy sediment” (*sensu* James, 2020) related to the formation of massive alluvial deposits in the valley floor needs also to be considered. These alluvial stores may have a long-term impact on the sediment supply of the rivers, and subsequently on the recovered channel morphology, that could be different from the pre-storm

conditions. It is possible that the recovered active channel width will be higher than that before the storm during decades. This will also depend on the controlling effects of extensive flood-protection works that have been done after the storm (dredging, bank protection works, earthworks in the valley floor), and it will be quite difficult to untangle natural processes of channel recovery from those related to massive protective operations in the valley floor.

5.2. Fluvial metamorphosis and sediment wave

Although flood-induced fluvial metamorphosis has already been reported in alpine environments, case studies showing the formation of braided channels over several tens of kilometers, like for the Vésubie, are extremely rare. Very few analogs exist in the recent history of the French mountains, for instance since the beginning of the 20th century. The June 1957 flood that occurred in the Guil and Ubaye alpine valleys is one documented example of flood-induced braided channel "mega-formation" (Arnaud-Fassetta et al., 2005, Brousse et al., 2011). A similar phenomenon likely occurred during the October 1940 flood in the Têt and Tech valleys of the Eastern French Pyrenees (at least 840 mm of rain in 24 hours, Soutadé 1994), but data are missing for characterizing the pre-flood channel morphology of these rivers. Aerial photographs taken in 1941 however reveal the presence of wide braided channels along many reaches of both valleys (https://remonterletemps.ign.fr/). Case studies of flood-induced braiding formation outside France have been also reported, but they document localized braiding formation affecting short river lengths (Nardi and Rinaldi, 2015; Scorpio et al., 2018) or relatively small mountain streams (Brenna et al., 2023). It is likely that a major fluvial metamorphosis occurred after the August 2005 catastrophic flood in Austrian Tyrol, as suggested by the very high mean width ratio reported by Krapesch et al. (2011) for the 34-km surveyed reach of the Trisanna River, but no information was provided about braiding formation in this case study.

Storm Alex provides some elements for the identification of key processes associated with the rapid mega-formation of braided channels after extreme floods. Of particular importance are the sediment cascading effects that could explain the emergence of a continuous braided pattern along 35 km, like observed in the Vésubie valley. Although sediment supply from tributaries has been very high, it is not

765 really possible to explain the longitudinal extent of the fluvial metamorphosis by a prograding
766 sediment wave generated in upper valleys, e.g. from upstream of the Boréon – Upper Vésubie
767 confluence. Many evidences rather suggest that the fueling effect of sediment transport by alluvial
768 storage is likely the key mechanism by which the sediment wave was regenerated step by step along
769 the reach (Fig. 18 and 19). The sharp decline of many geomorphic indicators (width ratio, post-flood
770 confinement index, channel aggradation) downstream the gorges of the Vésubie suggests an
771 attenuation of the sediment wave in the gorges, which must be considered as segments where the
772 fuelling effect by erosion of the pre-existing alluvial storages could not occur. Some important
773 stripping effects of surficial deposits in the margins of the active channel have been documented by
774 topographic differencing, showing that fluvial erosion of alluvial fans, fluvio-glacial terraces, and
775 colluvium deposits at the foot of hillslopes strongly contributed to the regeneration of the sediment
776 wave along all the investigated stream reaches. This fuelling effect from lateral stripping of active
777 channel margins is estimated at 4.1 Mm^3, and it is almost three times more than sediment supply from
778 tributaries (1.5 Mm^3). Although this figure is very high, it certainly corresponds to a lower bound
779 estimate of the actual fuelling effect from the valley floor, because an early phase of massive erosion
780 of fluvial terraces and floodplains likely occurred before channel aggradation. This was for example
781 the case during a catastrophic flood that occurred in October 2011 in the Northern Apennines, where
782 floodplain stripping before the formation of boulder bars was clearly seen from video documentation
783 (Rinaldi et al., 2016). This early phase of massive erosion cannot be detected by topographic
784 differencing. However, ortho-images show in many places the stripping of riparian forests (and also
785 buildings) that were present on alluvial surfaces that became the post-flood active channel (Fig. 21).
786 Although some ortho-images clearly show that some riparian forests have been buried by overbank
787 gravel deposition, i.e. without preliminary erosion of the terrace, this situation is far from being
788 dominant in the valley, where most of the trees has been removed before gravel deposition. All these
789 elements strongly support the idea that the fuelling effect of alluvial storage is a key element for
790 understanding not only sediment transport processes during extreme floods (Tricart, 1960; Korup,
791 2012), but also associated geomorphic responses.
792

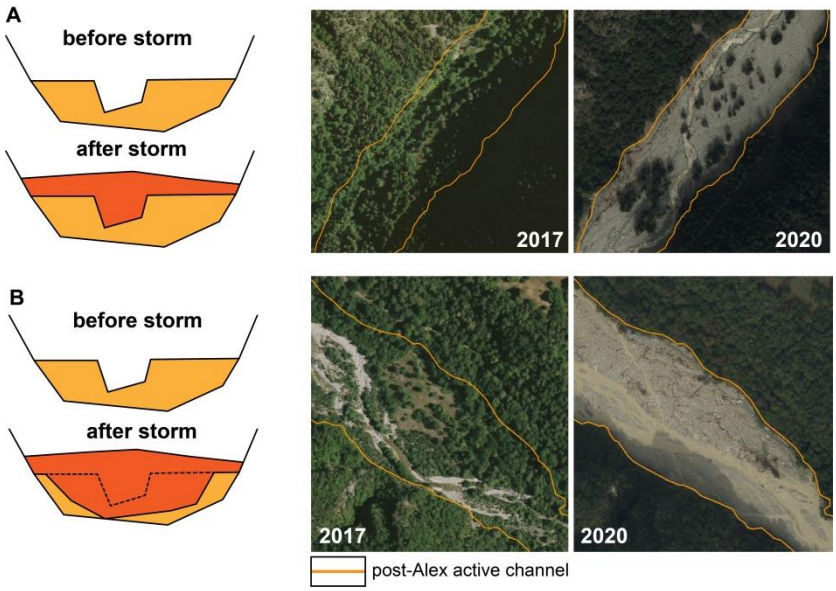

793

794 Figure 21. Schematic diagrams illustrating two types of channel aggradation mechanisms during Storm Alex.
795 (A) Overbank deposition of gravels (in orange) in the forested floodplain or fluvial terraces (in yellow) without
796 any early phase of erosion; this mechanism is attested by the persistence of the riparian forest in the post-flood
797 active channel. (B) Overbank deposition of gravels after an early phase of massive floodplain or terrace erosion;
798 this mechanism is attested by the stripping of the forest in the post-flood active channel; this situation was
799 dominant in the Vésubie valley after Storm Alex.

800

801 The catchment-scale sediment budget reconstructed for the Vésubie provides a sediment yield estimate
802 of 2.09 Mm^3. This estimate certainly incorporates an important fraction of suspended load, which
803 remains hard to evaluate. It has not been possible to undertake some grain-size distribution analysis for
804 eroded and deposited volumes included in the sediment budget, but it is likely that a differential of the
805 percentage of fines exists between eroded and deposited volumes, notably for tributaries. One reason
806 for this is that eroded volumes obtained for tributaries are mainly composed of remobilized colluvial
807 deposits with a supposedly high content of fines (e.g. sands coming from weathered granitic rocks,
808 silts and clays coming from marly rocks), while deposited volumes are made of gravel or boulder bars
809 along distal reaches, and debris-flow deposits on alluvial fans. This differential of fine fraction is
810 likely less important in the valley floor, since eroded and deposited volumes are mainly composed of
811 alluvial storages, even if some eroded colluvial deposits have been also incorporated in the valley floor
812 sediment budget. To illustrate the importance of this differential on sediment yield, a simple

calculation shows that a difference of only 20% (e.g. fine fraction of 40% for eroded volumes, vs. 20% for deposited volumes) reduces the sediment yield to only 380 000 m^3. Whatever the fine fraction of the sediment yield, it is clear that the suspended load of the Vésubie during Storm Alex has been extremely important, as suggested by the big turbidity plume that has been captured by satellite imagery in the Mediterranean Sea at the mouth of the Var River (Piton et al., 2024).

5.3. Implications for channel widening during catastrophic floods in alpine valleys

Recent literature on extreme-flood-related morphological adjustments in the Alps initially explores the link between stream power and channel widening in Austrian catchments (Krapesch et al., 2011), relying on Magilligan (1992) proposition of a 300 W m^{-2} threshold of specific stream power for major morphological adjustments to occur. Surian et al. (2016) and Righini et al. (2017) also stressed a significant effect of stream power on channel widening, with better results when the specific stream power is computed using the pre-flood channel width. This was later confirmed in two small catchments of Southwestern Germany (Lucia et al., 2018), where the authors were able to develop an explicit relationship between width ratio, specific stream power and confinement index, explaining 67% of the variability. Contemporary work in the Swiss pre-Alps (Ruiz-Villanueva et al., 2018) explores a wide range of controlling factors on channel widening, including for the first time not only hydraulic parameters, but also factors specifically linked to the triggering rainfall event. They highlight that models explain between 20% and 50% of channel widening variability, with the most significant variables being total maximum precipitation, stream power index and peak discharge. Recent works from Scorpio et al. (2018, 2022) in Italian catchments (Northern Apennines and South Tyrol) stressed the decisive role of valley confinement on channel adjustments, as well as flood power through both hydrological and hydraulic parameters. A preliminary analysis based on a simple stream power index computed for the Vésubie stream network shows encouraging results for the prediction of width ratios, provided that stream reaches classified as gorges are excluded (Fig. 17A). Further investigations are needed to integrate results from the hydrological modelling of Storm Alex for the computation of a distributed map of specific stream power along the stream network of both catchments (Payrastre et al., 2022). However, it clearly appears that Storm Alex channel adjustments

are not only controlled by hydraulic forces, but also by sediment supply. The positive correlation that we obtained between width ratios and bed-level changes strongly supports a strong sediment forcing on channel widening (Fig. 17C).

Knowledge about flood-induced active channel widening is crucial for determining a "safety space" or "freedom space" (Biron et al., 2014) for managing flooding hazard in alpine valleys. The documentation of Storm Alex active channel expansions provides a new dataset of width ratios associated with catastrophic floods having extreme return period in alpine environments. This dataset shows a 40% higher mean width ratio for the Vésubie as compared to the Roya, while hydro-meteorological forcings were more intense in the Roya catchment. This highlights the critical role of local conditions on channel response, the wider modern valley floor and residual alluvial storages of the Vésubie having clearly been favorable for active channel expansion. The limiting effect of channel confinement on width ratios, statistically confirmed for the Vésubie, has been also reported by several case studies (Surian et al., 2016; Righini et al., 2017; Lucia et al., 2018; Scorpio et al., 2018; Scorpio et al., 2022). All these studies found that the confinement index is a better predictor of channel widening than stream power, and our better correlation with the index confinement than with the stream power index agree with this result. The strong controlling effect of confinement during Storm Alex is also illustrated by the fact that along most of the upper confined reaches, active channel widening occurred over almost the entire modern valley floor, or even over a greater width than that of the pre-flood valley floor by eroding hillslope toe. This has strong implications for flood risk management in confined alpine valleys, where the entire valley floor should be considered as a potential zone of active channel expansion, as already shown during an extreme flood that occurred in the Apennines in October 2011 (Rinaldi et al., 2016; Surian et al., 2016).

Storm Alex also confirms a much higher geomorphic sensitivity for reaches having a narrow active channel before the flood, as previously reported by many case studies (Fig. 16). This means that narrow single-thread channels located in wide floodplains of alpine valleys should be considered as particularly sensitive zones for active channel expansion, even though the available space in the

nearby floodplain may be of interest for development and urbanization. The compilation of data on width ratios during extreme floods is helpful for determining an upper envelope of maximum potential active channel widening simply based on the initial width, and data points from the Vésubie clearly help to determine this upper envelope. It is interesting to see that maximum width ratios observed in the Vésubie are not outside the scatterplot of documented extreme floods in European upland rivers and streams (Fig. 16). This means that this scatterplot likely integrate enough variability for predicting the most extreme flood-induced geomorphic responses of temperate upland environments.

6. Conclusion

The reconstruction of geomorphic responses of two confined alpine valleys of the Southeastern French Alps following Storm Alex (October 2020) shows a quasi-continuous fluvial metamorphosis along the investigated stream networks, with dramatic active channel widening and aggradation, having no antecedent analogs during the last 70 years in both valleys. The different glacial imprints between the two valleys is considered a key factor explaining the exacerbated channel response in the Vésubie, where a braided channel emerged along a 35 km river length. Many evidences strongly support the idea that the fuelling effect of alluvial storage is a key element of the sediment cascade at the origin of the braided channel formation. While hydro-meteorological forcings were more intense in the Roya, a much higher active channel widening was observed in the Vésubie, its wider modern valley floor having clearly be favorable for active channel expansion. The strong controlling effect of confinement is illustrated by the fact that along most of the upper confined reaches, active channel widening occurred over the entire modern valley floor, or even over a greater width than that of the pre-flood valley floor by eroding hillslope toe. This has strong implications for flood risk management in confined alpine valleys, where the entire valley floor should be considered as a potential zone of active channel expansion during extreme events.

Acknowledgements

This study was supported by the *Direction Générale de la Prévention des Risques* (DGPR) of the French Ministry of Environment, by the EU Interreg-Alcotra RITA project (grant agreement n.8504),

and by the Université Côte d'Azur through the "Crédits Scientifiques Incitatifs 2021 - volet Recherche" funding call. ONF-RTM 06, Météo France, IGN, CEREMA, Métropole de Nice, and Pierre Brigode (Univ. Côte d'Azur) are acknowledged for the support in data sharing and general discussions and exchanges during post-flood surveys of Storm Alex. This work was performed in the framework of the LTER CNRS-INEE-ZABR (*Zone Atelier Bassin du Rhône*). Special thanks to Mélissandre who started the active channel mapping of the Vésubie during her "stage de 3e". This paper benefited from comments of two anonymous reviewers.

References

Alber A, Piégay H. 2011. Spatial disaggregation and aggregation procedures for characterizing fluvial features at the network-scale: application to the Rhône basin (France). Geomorphology 125: 343-360 https://doi.org/10.1016/j.geomorph.2010.09.009

Anderson SW. 2019. Uncertainty in quantitative analyses of topographic change: error propagation and the role of thresholding. Earth Surface Processes and Landforms 44: 1015-1033. https://doi.org/10.1002/esp.4551

Arnaud-Fassetta G, Fort M. 2004. La part respective des facteurs hydroclimatiques et anthropiques dans l'évolution récente (1956-2000) de la bande active du Haut-Guil, Queyras, Alpes françaises du Sud. Méditerranée 102: 143-156. https://doi.org/10.3406/medit.2004.3350

Arnaud-Fassetta, G., Cossart, E. and Fort, M., 2005. Hydro-geomorphic hazards and impact of man-made structures during the catastrophic flood of June 2000 in the Upper Guil catchment (Queyras, Southern French Alps). Geomorphology, 66: 41-67. https://doi.org/10.1016/j.geomorph.2004.03.014

Baker, V.R., Costa, J.E., 1987. Flood power. In: L. Mayer and D. Nash (Editors), Catastrophic Flooding. Allen and Unwin, Boston, pp. 1-21.

Beschta, R.L., 1983. Channel changes following storm-induced hillslope erosion in the Upper Kowai Basin, Torlesse Range, New Zealand. Journal of Hydrology (New Zealand) 22: 93-111.

Biron PM, Buffin-Bélanger T, Larocque M, Choné G, Cloutier C-A, Ouellet M-A, Demers S, Olsen T, Desjarlais C, Eyquem J. 2014. Freedom Space for Rivers: A Sustainable Management Approach to Enhance River Resilience. Environmental Management 54 : 1056–1073. https://doi.org/10.1007/s00267-014-0366-z

Blanchet J, Blanc A, Creutin JD. 2021a. Explaining recent trends in extreme precipitation in the Southwestern Alps by changes in atmospheric influences. Weather and Climate Extremes 33: 100356. https://doi.org/10.1016/j.wace.2021.100356

Blanchet J, Creutin JD, Blanc A. 2021b. Retreating winter and strengthening autumn Mediterranean influence on extreme precipitation in the Southwestern Alps over the last 60 years. Environmental Research Letters 16: 034056. https://doi.org/10.1088/1748-9326/abb5cd

Blanpied, J., Carozza, J.M. and Antoine, J.M., 2018. La connectivité sédimentaire dans la haute chaîne pyrénéenne par l'analyse de la crue de juin 2013: le rôle des formations superficielles. Géomorphologie: Relief, processus, environnement, 24(4): 389-402. https://doi.org/10.4000/geomorphologie.12718

Bravard, J.P., 1989. La métamorphose des rivières des Alpes françaises à la fin du Moyen-Age et à l'époque Moderne. Bulletin de la Société Géographique de Liège 25: 145-157.

Brenna A, Marchi L, Borga M, Ghinassi M, Zaramella M, Surian N. 2021. Sediment-water flows in mountain catchments: insights into transport mechanisms as responses to high-magnitude hydrological events. Journal of Hydrology 602: 126716. https://doi.org/10.1016/j.jhydrol.2021.126716

Brenna A, Marchi L, Borga M, Zaramella M, Surian N. 2023. What drives major channel widening in mountain rivers during floods? The role of debris floods during a high-magnitude event. Geomorphology 430: 108650. https://doi.org/10.1016/j.geomorph.2023.108650

Brousse G, Arnaud-Fassetta G, Cordier S. 2011. Evolution hydrogéomorphologique de la bande active de l'Ubaye (Alpes françaises du Sud) de 1956 à 2004 : contribution à la gestion des crues. Géomorphologie : relief, processus, environnement 17 : 307–318. https://doi.org/10.4000/geomorphologie.9510

948 Brunsden, D., 2001. A critical assessment of the sensitivity concept in geomorphology. Catena, 42:
949 99-123. https://doi.org/10.1016/S0341-8162(00)00134-X

950 Carley JK, Pasternack GB, Wyrick JR, Barker JR, Bratovich PM, Massa DA, Reedy GD, Johnson TR.
951 2012. Significant decadal channel change 58-67 years post-dam accounting for uncertainty in
952 topographic change detection between contour maps and point cloud models. Geomorphology 179:
953 71-88. https://doi.org/10.1016/j.geomorph.2012.08.001

954 Carrega, P. and Michelot, N., 2021. Une catastrophe hors norme d'origine météorologique le 2 octobre
955 2020 dans les montagnes des Alpes-Maritimes. Physio-Géo, 16: 1-75. https://doi.org/10.4000/physio-
956 geo.12370

957 Cenderelli, D.A. and Wohl, E.E., 2003. Flow hydraulics and geomorphic effects of glacial-lake
958 outburst floods in the Mount Everest region, Nepal. Earth Surface Processes and Landforms, 28: 385-
959 407. https://doi.org/10.1002/esp.448

960 Cerema. 2021. RETEX technique Alex: inondations des 2 et 3 octobre 2020, consensus hydrologique.
961 Unpublished technical report, Cerema, 59 pp.

962 Church M, Jakob M. 2020. What Is a Debris Flood? Water Resources Research 56: e2020WR027144.
963 https://doi.org/10.1029/2020WR027144

964 Comiti F. 2012. How natural are Alpine mountain rivers? Evidence from the Italian Alps. Earth
965 Surface Processes and Landforms 37: 693-707. https://doi.org/10.1002/esp.2267

966 Costa, J.E. and O'Connor, J.E., 1995. Geomorphically effective floods. Natural and Anthropogenic
967 Influences in Fluvial Geomorphology, AGU, Geophysical Monograph, 89: 45-56.

968 Croke J, Todd P, Thompson C, Watson F, Denham R, Khanal G. 2013. The use of multi temporal
969 LiDAR to assess basin-scale erosion and deposition following the catastrophic January 2011 Lockyer
970 flood, SE Queensland, Australia. Geomorphology 184: 111-126.
971 https://doi.org/10.1016/j.geomorph.2012.11.023

972 Fryirs K. 2013. (Dis)Connectivity in catchment sediment cascades: a fresh look at the sediment
973 delivery problem. Earth Surface Processes and Landforms 38: 30-46. https://doi.org/10.1002/esp.3242

Gomez B, Rosser BJ, Peacock DH, Hicks DM, Palmer JA. 2001. Downstream fining in a rapidly aggrading gravel bed river. Water Resources Research 37: 1813-1823. https://doi.org/10.1029/2001WR900007

Gomez B, Banbury K, Marden M, Trustrum NA, Peacock DH, Hoskin PJ. 2003. Gully erosion and sediment production: Te Weraroa Stream, New Zealand. Water Resources Research 39: 1187-1194. https://doi.org/10.1029/2002WR001342

Gottardi F, Obled C, Gailhard J, Paquet E. 2012. Statistical reanalysis of precipitation fields based on ground network data and weather patterns: Application over French mountains. Journal of Hydrology 432-433: 154-167. https://doi.org/10.1016/j.jhydrol.2012.02.014

Harvey AM. 2001. Coupling between hillslopes and channels in upland fluvial systems: implications for landscape sensitivity, illustrated from the Howgill Fells, northwest England. Catena 42: 225-250. https://doi.org/10.1016/S0341-8162(00)00139-9

Haschenburger JK, Cowie M. 2009. Floodplain stages in the braided Ngaruroro River, New Zealand. Geomorphology 103: 466-475. https://doi.org/10.1016/j.geomorph.2008.07.016

Heritage G, Entwistle N, Milan D, Tooth S. 2019. Quantifying and contextualising cyclone-driven, extreme flood magnitudes in bedrock-influenced dryland rivers. Advances in Water Resources 123: 145-159. https://doi.org/10.1016/j.advwatres.2018.11.006

James LA. 1991. Incision and morphologic evolution of an alluvial channel recovering from hydraulic mining sediment. Geological Society of America Bulletin 103: 723-736. https://doi.org/10.1130/0016-7606(1991)103%3C0723:IAMEOA%3E2.3.CO;2

James LA. 2010. Secular sediment waves, channel bed waves, and legacy sediment. Geography Compass 4: 576-598. https://doi.org/10.1111/j.1749-8198.2010.00324.x

Julian, M., 1997. Les glaciations des Alpes Maritimes: essai de mise au point. In: P. Pech, L. Simon and M. Tabeaud M (Editors), Géo-méditer Géographie physique et Méditerranée: Hommage à Gaston Beaudet et Etienne Moissenet. Editions de la Sorbonne, Paris, pp. 245-261.

999 Kochel, R.C., 1988. Geomorphic impact of large floods: review and new perspectives on magnitude
1000 and frequency. In: V.R. Baker, R.C. Kochel and P.C. Patton (Editors), Flood geomorphology. Wiley-
1001 Interscience, New York, pp. 169-187.

1002 Korup O. 2004. Landslide-induced river channel avulsions in mountain catchments of southwest New
1003 Zealand. Geomorphology 63: 57-80. https://doi.org/10.1016/j.geomorph.2004.03.005

1004 Korup, O., 2012. Earth's portfolio of extreme sediment transport events. Earth-Science Reviews,
1005 112(3–4): 115-125. https://doi.org/10.1016/j.earscirev.2012.02.006

1006 Krapesch, G., Hauer, C. and Habersack, H., 2011. Scale orientated analysis of river width changes due
1007 to extreme flood hazards. Natural Hazards and Earth System Sciences, 11(8): 2137-2147.
1008 https://doi.org/10.5194/nhess-11-2137-2011

1009 Lallias-Tacon S, Liébault F, Piégay H. 2014. Step by step error assessment in braided river sediment
1010 budget using airborne LiDAR data. Geomorphology 214: 307-323.
1011 https://doi.org/10.1016/j.geomorph.2014.02.014

1012 Lane SN, Westaway RM, Hicks DM. 2003. Estimation of erosion and deposition volumes in a large,
1013 gravel-bed, braided river using synoptic remote sensing. Earth Surface Processes and Landforms 28:
1014 249-271. https://doi.org/10.1002/esp.483

1015 Liébault F, Piégay H. 2002. Causes of 20th century channel narrowing in mountain and piedmont
1016 rivers of Southeastern France. Earth Surface Processes and Landforms 27: 425-444
1017 https://doi.org/10.1002/esp.328

1018 Liébault F, Gomez B, Page M, Marden M, Peacock D, Richard D, Trotter CM. 2005. Land-use
1019 change, sediment production and channel response in upland regions. River Research and Applications
1020 21: 739-756. https://doi.org/10.1002/rra.880

1021 Liébault, F., Piégay, H., Frey, P., Landon, N., 2008. Tributaries and the management of main-stem
1022 geomorphology. In River Confluences, Tributaries and the Fluvial Network, Rice SP, Roy A, Rhoads
1023 BL (eds). John Wiley and Sons: Chichester; 243-270.

1024 Liébault F, Lallias-Tacon S, Cassel M, Talaska N. 2013. Long profile responses of alpine braided
1025 rivers in SE France. River Research and Applications 29: 1253-1266. https://doi.org/10.1002/rra.2615.

1026 Lucía, A., Schwientek, M., Eberle, J. and Zarfl, C., 2018. Planform changes and large wood dynamics
1027 in two torrents during a severe flash flood in Braunsbach, Germany 2016. Science of The Total
1028 Environment, 640-641: 315-326. https://doi.org/10.1016/j.scitotenv.2018.05.186

1029 Lun D, Fischer S, Viglione A, Blöschl G. 2020. Detecting Flood-Rich and Flood-Poor Periods in
1030 Annual Peak Discharges Across Europe. Water Resources Research 56: e2019WR026575.
1031 https://doi.org/10.1029/2019WR026575

1032 Madej MA, Ozaki V. 1996. Channel response to sediment wave propagation and movement, Redwood
1033 Creek, California, USA. Earth Surface Processes and Landforms 21: 911-927.
1034 https://doi.org/10.1002/(SICI)1096-9837(199610)21:10%3C911::AID-ESP621%3E3.0.CO;2-1

1035 Magilligan FJ. 1992. Thresholds and the spatial variability of flood power during extreme floods.
1036 Geomorphology 5: 373-390. https://doi.org/10.1016/0169-555X(92)90014-F

1037 Magilligan FJ, Phillips JD, James LA, Gomez B. 1998. Geomorphic and sedimentological controls on
1038 the effectiveness of an extreme flood. Journal of Geology 106: 87-95. https://doi.org/10.1086/516009

1039 Magilligan, F.J., Gomez, B., Mertes, L.A.K., Smith, L.C., Smith, N.D., Finnegan, D. and Garvin, J.B.,
1040 2002. Geomorphic effectiveness, sandur development, and the pattern of landscape response during
1041 jökulhlaups: SkeiOararsandur, southeastern Iceland. Geomorphology, 44: 95-113.
1042 https://doi.org/10.1016/S0169-555X(01)00147-7

1043 Marutani T, Kasai M, Reid LM, Trustrum NA. 1999. Influence of storm-related sediment storage on
1044 the sediment delivery from tributary catchments in the Upper Waipaoa River, New Zealand. Earth
1045 Surface Processes and Landforms 24: 881-896. https://doi.org/10.1002/(SICI)1096-
1046 9837(199909)24:10%3C881::AID-ESP17%3E3.0.CO;2-I

1047 Milan, D.J., 2012. Geomorphic impact and system recovery following an extreme flood in an upland
1048 stream: Thinhope Burn, northern England, UK. Geomorphology, 138(1): 319-328.
1049 https://doi.org/10.1016/j.geomorph.2011.09.017

1050 Milan DJ, Heritage G, Tooth S, Entwistle N. 2018. Morphodynamics of bedrock-influenced dryland
1051 rivers during extreme floods: Insights from the Kruger National Park, South Africa. Bulletin of the
1052 Geological Society of America 130: 1825-1841. https://doi.org/10.1130/B31839.1

1053 Milan DJ. 2022. Modelling differential geomorphic effectiveness in neighbouring upland catchments:
1054 implications for sediment and flood risk management in a wetter world. Progress in Physical
1055 Geography: Earth and Environment 46: 124-151. https://doi.org/10.1177/03091333211045514

1056 Nanson GC. 1986. Episodes of vertical accretion and catastrophic stripping: a model of disequilibrium
1057 flood-plain development. Geological Society of America Bulletin 97: 1467-1475.
1058 https://doi.org/10.1130/0016-7606(1986)97%3C1467:EOVAAC%3E2.0.CO;2

1059 Nardi L, Rinaldi M. 2015. Spatio-temporal patterns of channel changes in response to a major flood
1060 event: the case of the Magra River (central-northern Italy). Earth Surface Processes and Landforms 40:
1061 326-339. https://doi.org/10.1002/esp.3636

1062 Nelson, A. and Dubé, K., 2016. Channel response to an extreme flood and sediment pulse in a mixed
1063 bedrock and gravel-bed river. Earth Surface Processes and Landforms, 41(2): 178-195.
1064 https://doi.org/10.1002/esp.3843

1065 Nyberg B, Buckley SJ, Howell JA, Nanson RA. 2015. Geometric attribute and shape characterization
1066 of modern depositional elements: A quantitative GIS method for empirical analysis. Computers &
1067 Geosciences 82: 191-204. https://doi.org/10.1016/j.cageo.2015.06.003

1068 ONF-RTM-INRAE, 2022a. Retour d'expérience technique de la crue du 2 octobre 2020 dans la vallée
1069 de la Vésubie, volet torrentiel. Unpublished technical report, Ministère de la Transition Ecologique,
1070 Direction Départementales des Territoires et de la Mer, 300 pp. https://doi.org/10.57745/UGJZWT

1071 ONF-RTM-INRAE, 2022b. Retour d'expérience technique de la crue du 2 octobre 2020 dans la vallée
1072 de la Roya, volet torrentiel. Unpublished technical report, Ministère de la Transition Ecologique,
1073 Direction Départementales des Territoires et de la Mer, 275 pp. https://doi.org/10.57745/B69M2O

1074 Payrastre O, Nicolle P, Bonnifait L, Brigode P, Astagneau P, Baise A, Belleville A, Bouamara N,
1075 Bourgin F, Breil P, Brunet P, Cerbelaud A, Courapied F, Devreux L, Dreyfus R, Gaume E, Nomis S,

Poggio J, Pons F, Rabab Y, Sevrez D. 2022. The 2 October 2020 Alex storm in south-eastern France: a contribution of the scientific community to the flood peak discharges estimation. LHB Hydroscience Journal: 2082891. https://doi.org/10.1080/27678490.2022.2082891

Pellegrini G, Martini L, Cavalli M, Rainato R, Cazorzi A, Picco L. 2021. The morphological response of the Tegnas alpine catchment (Northeast Italy) to a Large Infrequent Disturbance. Science of The Total Environment 770: 145209. https://doi.org/10.1016/j.scitotenv.2021.145209

Piégay H, Darby SE, Mosselman E, Surian N. 2005. A review of techniques available for delimiting the erodible river corridor: a sustainable approach to managing bank erosion. River Research and Applications 21: 773-789. https://doi.org/10.1002/rra.881

Pitlick, J., 1993. Response and recovery of a subalpine stream following a catastrophic flood. Geological Society of America Bulletin, 105: 657-670. https://doi.org/10.1130/0016-7606(1993)105%3C0657:RAROAS%3E2.3.CO;2

Piton G, Carladous S, Recking A, Tacnet JM, Liébault F, Kuss D, Quefféléan Y, Marco O. 2017. Why do we build check dams in Alpine streams? An historical perspective from the French experience. Earth Surface Processes and Landforms 42: 91-108. https://doi.org/10.1002/esp.3967

Piton G, Cohen M, Flipo M, Nowak M, Chapuis M, Melun G, Robert Y, Andréis N, Liébault F. 2024. Large in-stream wood yield during an extreme flood (Storm Alex, October 2020, Roya Valley, France): Estimating the supply, transport, and deposition using GIS. Geomorphology 446: 108981. https://doi.org/10.1016/j.geomorph.2023.108981

Rainato R, Martini L, Pellegrini G, Picco L. 2021. Hydrological, geomorphic and sedimentological responses of an alpine basin to a severe weather event (Vaia storm). CATENA 207: 105600. https://doi.org/10.1016/j.catena.2021.105600

Righini, M., Surian, N., Wohl, E., Marchi, L., Comiti, F., Amponsah, W. and Borga, M., 2017. Geomorphic response to an extreme flood in two Mediterranean rivers (northeastern Sardinia, Italy): analysis of controlling factors. Geomorphology, 290: 184-199. https://doi.org/10.1016/j.geomorph.2017.04.014

Rinaldi, M., Amponsah, W., Benvenuti, M., Borga, M., Comiti, F., Lucía, A., Marchi, L., Nardi, L., Righini, M. and Surian, N., 2016. An integrated approach for investigating geomorphic response to extreme events: methodological framework and application to the October 2011 flood in the Magra River catchment, Italy. Earth Surface Processes and Landforms, 41(6): 835-846. https://doi.org/10.1002/esp.3902

Ruiz-Villanueva, V., Badoux, A., Rickenmann, D., Böckli, M., Schläfli, S., Steeb, N., Stoffel, M. and Rickli, C., 2018. Impacts of a large flood along a mountain river basin: the importance of channel widening and estimating the large wood budget in the upper Emme River (Switzerland). Earth Surface Dynamics, 6(4): 1115-1137. https://doi.org/10.5194/esurf-6-1115-2018

Roussel, J.R., Auty, D., Coops, N. C., Tompalski, P., Goodbody, T. R. H., Sánchez Meador, A., Bourdon, J.F., De Boissieu, F., Achim, A. 2020. lidR : An R package for analysis of Airborne Laser Scanning (ALS) data. Remote Sensing of Environment, 251: 112061. https://doi:10.1016/j.rse.2020.112061

Schumm SA. 1969. River metamorphosis. American Society of Civil Engineers, Journal of the Hydraulics Division 95: 255-273. https://doi.org/10.1061/JYCEAJ.0001938

Scorpio V, Crema S, Marra F, Righini M, Ciccarese G, Borga M, Cavalli M, Corsini A, Marchi L, Surian N, Comiti F. 2018. Basin-scale analysis of the geomorphic effectiveness of flash floods: a study in the northern Apennines (Italy). Science of The Total Environment 640-641: 337-351. https://doi.org/10.1016/j.scitotenv.2018.05.252

Scorpio, V., Cavalli, M., Steger, S., Crema, S., Marra, F., Zaramella, M., Borga, M., Marchi, L. and Comiti, F., 2022. Storm characteristics dictate sediment dynamics and geomorphic changes in mountain channels: A case study in the Italian Alps. Geomorphology, 403: 108173. https://doi.org/10.1016/j.geomorph.2022.108173

Soutadé, G., 1994. Les inondations d'octobre 1940 dans les Pyrénées Orientales d'après les rapports adressés à M. Pardé par les instituteurs. Dossier de la Revue de Géographie Alpine 12: 131-134.

Surian, N., Righini, M., Lucía, A., Nardi, L., Amponsah, W., Benvenuti, M., Borga, M., Cavalli, M., Comiti, F., Marchi, L., Rinaldi, M. and Viero, A., 2016. Channel response to extreme floods: Insights on controlling factors from six mountain rivers in northern Apennines, Italy. Geomorphology, 272: 78-91. https://doi.org/10.1016/j.geomorph.2016.02.002

Tramblay Y, Mimeau L, Neppel L, Vinet F, Sauquet E. 2019. Detection and attribution of flood trends in Mediterranean basins. Hydrology and Earth System Sciences 23: 4419-4431. https://doi.org/10.5194/hess-23-4419-2019

Tricart, J., 1960. Mécanismes normaux et phénomènes catastrophiques dans l'évolution des versants du bassin du Guil (Hautes-Alpes, France). Zeitschrift für Geomorphologie, 5/4: 227-301.

Williams, P.F., Rust, B.R., 1969. The sedimentology of a braided river. Journal of Sedimentary Petrology 39: 649-679.

Wolman MG, Gerson R. 1978. Relative scales of time and effectiveness of climate in watershed geomorphology. Earth Surface Processes and Landforms 3: 189-208. https://doi.org/10.1002/esp.3290030207